



Pan-Antarctic map of near-surface permafrost temperatures at 1 km² scale

Jaroslav Obu¹, Sebastian Westermann¹, Gonçalo Vieira², Andrey Abramov³, Megan Balks⁴, Annett Bartsch^{5,6}, Filip Hrbáček⁷, Andreas Kääh¹, Miguel Ramos⁸

¹Department of Geosciences, University of Oslo, Oslo, Sem Sælands vei 1, 0371 Oslo, Norway

²Centre of Geographical Studies, Institute of Geography and Spatial Planning, University of Lisbon, R. Branca Edmée Marques, 1600-276 Lisbon, Portugal

10 ³Institute of Physicochemical and Biological Problems in Soil Science, Russian Academy of Sciences, Pushchino, Russia

⁴Department of Earth and Ocean Sciences, University of Waikato, Hamilton, Private Bag 3105, New Zealand

⁵Zentralanstalt für Meteorologie und Geodynamik, Hohe Warte 39, Vienna, Austria

⁶now at b.geos GmbH, Vienna, Industriestrasse 1 2100 Korneuburg, Austria

⁷Department of Geography, Masaryk University, Kotlářská 2 61137 Brno, Czech Republic

15 ⁸Department of Physics and Mathematics, University of Alcalá, Madrid, Campus universitario 28805 Alcalá de Henares, Spain

Correspondence to: Jaroslav Obu (jaroslav.obu@geo.uio.no)

Abstract

20 Permafrost is present under almost all of the Antarctic's ice-free areas but little is known about spatial variations of permafrost temperatures outside a few areas with established ground temperature measurements. We modelled a temperature at the top of the permafrost (TTOP) for all the ice-free areas of Antarctic mainland and Antarctic Islands at 1 km² resolution during 2000–2017. The model was driven by remotely-sensed land surface temperatures and down-scaled ERA-Interim climate reanalysis data and subgrid permafrost variability was simulated by variable snow cover. The results were validated against in-situ
25 measured ground temperatures from 40 permafrost boreholes and the resulting root mean square error was 1.9 °C. The lowest near-surface permafrost temperature of -33 °C was modelled at Mount Markham in Queen Elizabeth Range in the Transantarctic Mountains. This is the lowest permafrost temperature on Earth according to the modelling results on global scale. The temperatures were most commonly modelled between -23 and -18 °C for mountainous areas rising above the Antarctic Ice Sheet and between -14 and -8 °C for coastal areas. The model performance was good where snow conditions
30 were modelled realistically but errors of up to 4 °C can occur at sites with strong wind-driven redistribution of snow.



1 Introduction

Permafrost in the Antarctic is present beneath all ice-free terrain, except for the lowest elevations of the maritime Antarctic and sub-Antarctic islands (Vieira et al., 2010), unlike the northern hemisphere, where permafrost underlies approximately 15 % of the unglaciated land. The ice and snow-free land occupies 0.22% (30 900 km²) of the whole Antarctic (Burton-Johnson et al., 2016; Hrbáček et al., 2018). The major ice-free areas include the Queen Maud Land, Enderby Land, the Vestfold Hills, Wilkes Land, the Transantarctic Mountains, the Ellsworth Mountains, Marie Byrd Land and the Antarctic Peninsula (Green et al., 1967; Fig. 1). Despite the relatively small area, in comparison to glaciated areas, permafrost is one of the major factors controlling terrestrial ecosystem dynamics in the Antarctic (Bockheim et al., 2008).

10 Compared with the Northern Hemisphere, where the first permafrost investigations date back to 19th century (Shiklomanov, 2005; Humlum et al., 2016), the ground temperatures in the Antarctic have been systematically studied only during the last two decades. Permafrost was studied in relation to patterned ground since the 1960s and during the Dry Valley Drilling Project in the 1970s but temperatures have been measured only occasionally (Decker and Bucher, 1977; Guglielmin, 2012). A first Antarctic permafrost borehole network was implemented in 1999 in the Victoria Land (Transantarctic Mountains) and was
15 extended during the International Polar Year 2007–2009 to cover all eight major ice-free regions (Vieira, 2010).

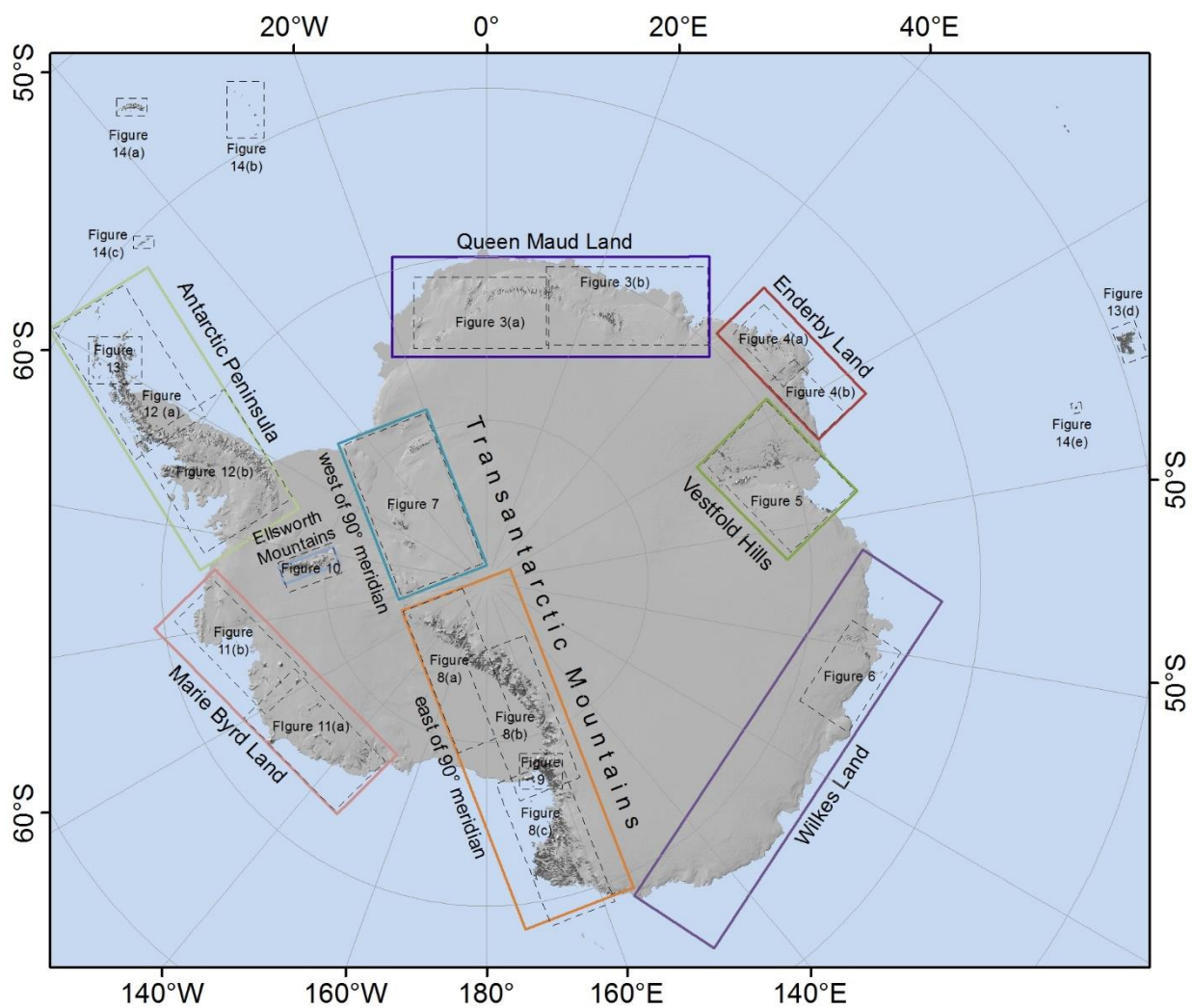
Permafrost distribution was estimated and mapped on the Antarctic Peninsula by Bockheim et al. (2013) based on mean annual temperature, periglacial features, shallow excavations, borehole measurements, geophysical surveys, and existing permafrost models. Bockheim et al. (2007) characterised permafrost in the McMurdo Dry Valleys based on ground ice properties and
20 active layer thickness from more than 800 shallow excavations.

Antarctic permafrost modelling efforts were limited to small areas in the Antarctic Peninsula region and sub-Antarctic Islands. Ferreira et al. (2017) used freezing indexes and the temperature at the top of the permafrost (TTOP) modelling for eight monitored sites on Hurd Peninsula, Livingston Island for the 2007 and 2009 seasons to study the controlling factors of ground
25 temperatures. Rocha et al., (2010) ran the H-TESSSEL scheme forced by ERA-Interim reanalysis to simulate ground temperatures at Reina Sofia Peak on Livingston Island. Ground temperature measurements and permafrost modelling efforts have been limited to point sites and little is known about spatial variability of ground temperatures at the regional and continent-wide scales.

30 In this study we employed the TTOP modelling scheme based on The Moderate Resolution Imaging Spectroradiometers (MODIS) land surface temperatures (LST) and ERA-Interim reanalysis to model the spatial distribution of temperatures at the top of permafrost on all ice-free areas of Antarctic and Antarctic Islands. We adapt the existing modelling scheme from the



Northern Hemisphere (Westermann et al., 2015; Obu et al., 2019) according to the available input data and their characteristics for the Antarctic.



5 Figure 1: Overview map of the ice-free Antarctic regions and extents of the maps presented in the paper.



2 Methods

2.1 The Cryogrid 1 model

The CryoGrid 1 model (Gisnås et al., 2013) calculates mean annual ground temperature (MAGT) and is based on the TTOP equilibrium approach (Smith and Riseborough, 1996):

5

$$MAGT = \begin{cases} \frac{1}{\tau} (n_f FDD + r_k n_t TDD) \\ \text{for } (n_f FDD + r_k n_t TDD) \leq 0 \\ \frac{1}{\tau} \left(\frac{1}{r_k} n_f FDD + n_t TDD \right) \\ \text{for } (n_f FDD + r_k n_t TDD) > 0 \end{cases}$$

Where: FDD and TDD represent freezing and thawing degree days, respectively, of the surface meteorological forcing accumulated over the model period τ in days. The influence of the seasonal snow cover, vegetation, and ground thermal properties were taken into account by the semi-empirical adjustment factors r_k (ratio of thermal conductivity of the active layer in thawed and frozen state), n_f (scaling factor between average winter surface and ground surface temperature) and n_t (scaling factor between average summer surface and ground surface temperature). We use land surface temperature (LST) to compute FDD and TDD (see following section) instead of the air temperature that was used initially by Smith and Riseborough (2002) and hence omit thawing n_t -factors.

15

2.2 Freezing and thawing degree days

Spatially distributed data sets of TDD and FDD were compiled from remotely sensed land surface temperature products and climate reanalysis data following the procedure of Obu et al. (2019). We used LST data (level 3 product in processing version 6) from MODIS on board the Terra and Aqua satellites, which contain up to two daytime and two night-time measurements per day at a spatial resolution of 1 km since the year 2000 (Wan, 2014). For this reason, the study extends from 2000 and to the end of 2017. Data gaps in the MODIS LST time series due to cloud cover can result in a systematic cold bias in seasonal averages (Westerman et al., 2012; Soliman et al., 2012; Østby et al., 2014), so a gap filling with near-surface air temperatures from the ERA-interim and ERA-5 reanalysis was applied (Westermann et al., 2015).

25

The ERA-interim reanalysis provides gap-free meteorological data from 1979 onwards at a spatial resolution of $0.75^\circ \times 0.75^\circ$ (Dee et al., 2011). The ERA-5 reanalysis is ERA-Interim upgrade and provides the data at improved $0.28125^\circ \times 0.28125^\circ$ (31 km) spatial resolution but was at the time of the study available only from 2008 onwards (Hersbach and Dee, 2016). ERA-



Interim data were for this reason used before 2008 and ERA-5 data afterwards. The reanalysis data were downscaled to the 1 km resolution of individual MODIS pixels using atmospheric lapse rates and The Global Multi-resolution Terrain Elevation Data 2010 (GMTED2010) (Danielson and Gesch, 2011). The downscaling methodology is described in detail by Fiddes and Gruber (2014), Westermann et al. (2015) and Obu et al. (2019). The gap-filled MODIS LST time series were averaged to eight-day periods from which FDD and TDD were finally accumulated for the 2000–2017 study period.

2.3 Average annual snowfall and n_f -factors

Spatially distributed data sets of n_f -factors were generated from average annual snowfall forced by ERA-Interim and ERA-5 reanalysis data. Snow cover in the majority of the Antarctic is dominated by sublimation and processes related to blowing snow (Gallée, 1998; Bintanja and Reijmer, 2001), which were not taken in to account by the snowfall and degree-day model that Obu et al. (2019) used to estimate n_f -factor for the Northern Hemisphere. For this reason, only mean annual snowfall was calculated using downscaled ERA-Interim precipitation before 2008 and ERA-5 precipitation after. Precipitation was downscaled based on the difference between reanalysis elevation and GMTED2010 using a precipitation gradient, found in drier areas (Hevesi et al., 1992), of 2 % per 100 m up to 1000 m and 1% per 100 m for elevations above 1000 m. Snowfall was defined as precipitation at air temperatures below 0 °C, using the downscaled ERA-Interim air temperatures as employed for the gap filling of MODIS LST (see above). For a detailed downscaling procedure description see Obu et al. (2019).

N_f -factors were defined based on average annual snowfall, however the reported n_f -factors in Antarctic were calculated in respect to snow depth. Oliva et al. (2017) identified n_f -factor values around 0.3 for snow accumulations of 80 cm on Livingston Island, although the n_f -factors can reach up to 0.55 in the thick snow cover due to its temporal variability (de Pablo et al., 2017). N_f -factors close to, or even greater than, one were measured in areas with little or no snow cover on Veleskarvet nunatak (Kotzé and Meiklejohn, 2017), in the McMurdo Dry Valleys (Lacelle et al., 2016) and on James Ross Island (Hrbáček et al., 2016). This range was used to constrain the n_f -factor ranges in relation to average annual snowfall (Table 1). Since the snow model was not able to simulate snow free-sites nor snowdrifts due to strong wind distribution, we used a maximum n_f -factor of 0.95 and minimum of 0.3. However, smaller snow-depth variations on a local scale were taken into account with an ensemble of different values of average annual snowfall for each 1 km² pixel (e.g. Gislås et al., 2014).



Mean annual snowfall (mm)	n_f min	n_f max
< 3	0.85	0.95
3-10	0.77	0.85
10-30	0.75	0.77
30-50	0.73	0.75
50-75	0.67	0.73
75-100	0.64	0.67
100-125	0.55	0.64
125-150	0.5	0.55
150-200	0.45	0.5
200-300	0.4	0.45
> 300	0.3	0.4

Table 1: ranges of n_f -factors that were assigned to mean annual snowfall values.

2.4 r_k -factors

- 5 The r_k -factor is defined as the ratio of thawed and frozen thermal conductivities of the active layer material (Romanovsky and Osterkamp, 1995) and is related to water and organic contents (e.g. Gislås et al., 2013). Soil moisture properties were mapped on a regional scale (Bockheim et al., 2007) but no pan-Antarctic datasets related to soil water or organic contents were available. The ESA CCI Landcover that Obu et al. (2019) used for Northern Hemisphere contains only “permanent snow and ice” class on the Antarctic mainland, therefore, a rock outcrops dataset (Burton-Johnson et al., 2016) was used to constrain non-glaciated areas. An r_k -factor of 0.85 was used for the whole Antarctic, representing an average value between very dry sites on continental Antarctic and moderately moist sites on the Antarctic Peninsula.

2.5 Ensemble-based modelling of subpixel heterogeneity

- 15 Ground temperatures can vary considerably at short distances due to heterogeneous snow cover, vegetation, topography and soil properties (Beer, 2016; Gislås et al., 2014; 2016; Zhang et al., 2014). We ran an ensemble of 200 model realisations with different combinations of n_f - and r_k -factors to simulate the variability. R_k -factor values were set to randomly vary by ± 0.1 between 0.75 and 0.95 to represent both very dry sites and locations with higher soil moisture. The distribution of snowfall within the 1 km pixel was simulated using a log-normal distribution function where mean annual snowfall determined the mean of the distribution. The coefficient of variation of the distribution for the open areas (0.9) according to Liston (2004) was assigned to all modelled areas. An n_f -factor was assigned to the estimated average annual snowfall according to Table 1. The



pixels not overlapping with rock outcrops were masked out. A fraction of model runs with $MAGT < 0\text{ }^{\circ}\text{C}$ was used to derive permafrost type (zones) on Antarctic Islands (see Obu et al. (2019) for detailed description).

2.6 Model validation

We compared our results to available in-situ measurements in 40 permafrost boreholes and shallow boreholes at soil-climate stations. The ensemble mean of modelled MAGTs was compared to the borehole measurements to take the simulated spatial variability, provided by the ensemble spread, into account. The accuracy of the model was estimated with root mean square error (RMSE) and mean absolute error between the modelled and measured MAGT.

The validation data were provided by the authors for the McMurdo Dry Valleys, ice-free areas near Russian stations (Bunger Hills, Schirmacher Hills, Larsemann Hills, Thala Hills, King George Island and Hobs coast) and the Northern Antarctic Peninsula. Ground temperatures from these locations represent mean MAGT at the top of the permafrost and usually overlap well with the modelling period 2000–2017 (Appendix A). Validation data for Queen Maud Land (Troll Station, Flarjuven Bluff, Vesleskarvet) and the Baker Rocks site were obtained from Hrbáček et al., (2018) and MAGTs from Terra Nova Bay (Oasi New and Boulder Clay) were obtained from Vieira et al., (2010). MAGTs from Hope Bay, Mt. Dolence, Marble Point Borehole and Limnopolar Lake were obtained from Schaefer et al. (2017a), Schaefer et al. (2017b), Guglielmin et al. (2011) and de Pablo et al. (2014), respectively. The borehole data from Signy Island and Rothera Point were extracted from Guglielmin et al., (2012) and (2014). The data found in publications were not necessarily calculated for the top of the permafrost and do not completely overlap with the modelling period and are, thus, less reliable than the author-supplied validation data. For instance, the data from Vieira et al. (2010) represents MAGT for the periods before 2010 usually lasting only few years (Table 2).

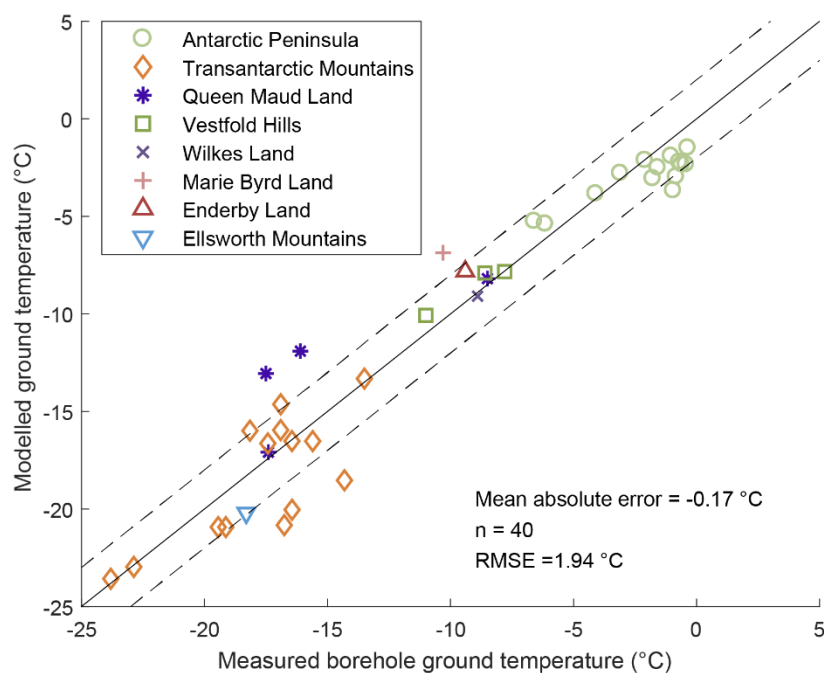
3 Results

3.1 Comparison to borehole measurements

Ground temperatures can vary significantly inside a 1 km^2 model pixel, which is, to a certain extent, represented by the TTOP model ensemble runs. Average MAGT derived from the ensemble runs was compared to the measured site ground temperatures, which might limit representativeness for sites with locally specific ground and snow properties. The comparison yielded a RMSE of $1.94\text{ }^{\circ}\text{C}$ and a mean absolute error for all boreholes of $0.06\text{ }^{\circ}\text{C}$ (Fig. 2). The small mean absolute error is partly achieved with fine adjustment of the n_f -factor class limits. For 50 % of the boreholes, the agreement between borehole temperatures and modelled MAGT was better than $1\text{ }^{\circ}\text{C}$, while it is better than $2\text{ }^{\circ}\text{C}$ for 75%, and better than $3\text{ }^{\circ}\text{C}$ for 85 % of the boreholes. Assuming a Gaussian distribution of standard deviation σ_{MAGT} , 68% of borehole comparisons should fall within one σ_{MAGT} , while 95% within two σ_{MAGT} , and 99% should be within three σ_{MAGT} . For the comparison with



Antarctic boreholes, 18 (45 %) boreholes were contained within one, 29 (73 %) within two, and 31 (78 %) within three standard deviations from the mean, which is comparable to the results for the Northern Hemisphere (Obu et al., 2019).



5

Figure 2: Measured vs. modelled permafrost temperatures for all boreholes. The dashed lines represent ± 2 °C intervals around the 1:1 solid line.

3.2 Queen Maud Land

- 10 There are 2430 km² of ice free areas in Queen Maud Land according to the rock outcrop map (Burton-Johnson et al., 2016; Hrbáček et al., 2018). The average MAGT is -18.2 °C and it ranges from -26.2 °C in the highest parts of Fimbulheimen Range to -6.3 °C in Prince Olav Coast, where MAGTs down to -10 °C were modelled at elevations exceeding 200 m (Fig. 3). MAGTs above -10 °C can be found also at Schirmacher Oasis (Hills) and reach above -8 °C. MAGTs in Sør Rondane Mountains and in Fimbulheimen Range range from -12 °C at elevations of around 800 m a.s.l. to -24 °C at elevations exceeding 3000 m a.s.l..
- 15 Kirwan Escarpment (elevations usually exceeding 2000 m) is characterised by MAGTs between -23 °C and -20 °C and in Heimefront Range (with slightly lower elevations) MAGTs were between -22 °C and -18 °C. MAGTs in Borg Massif were modelled from -21 to -17 °C and between -16 and -12 °C in Ahlmann Ridge.

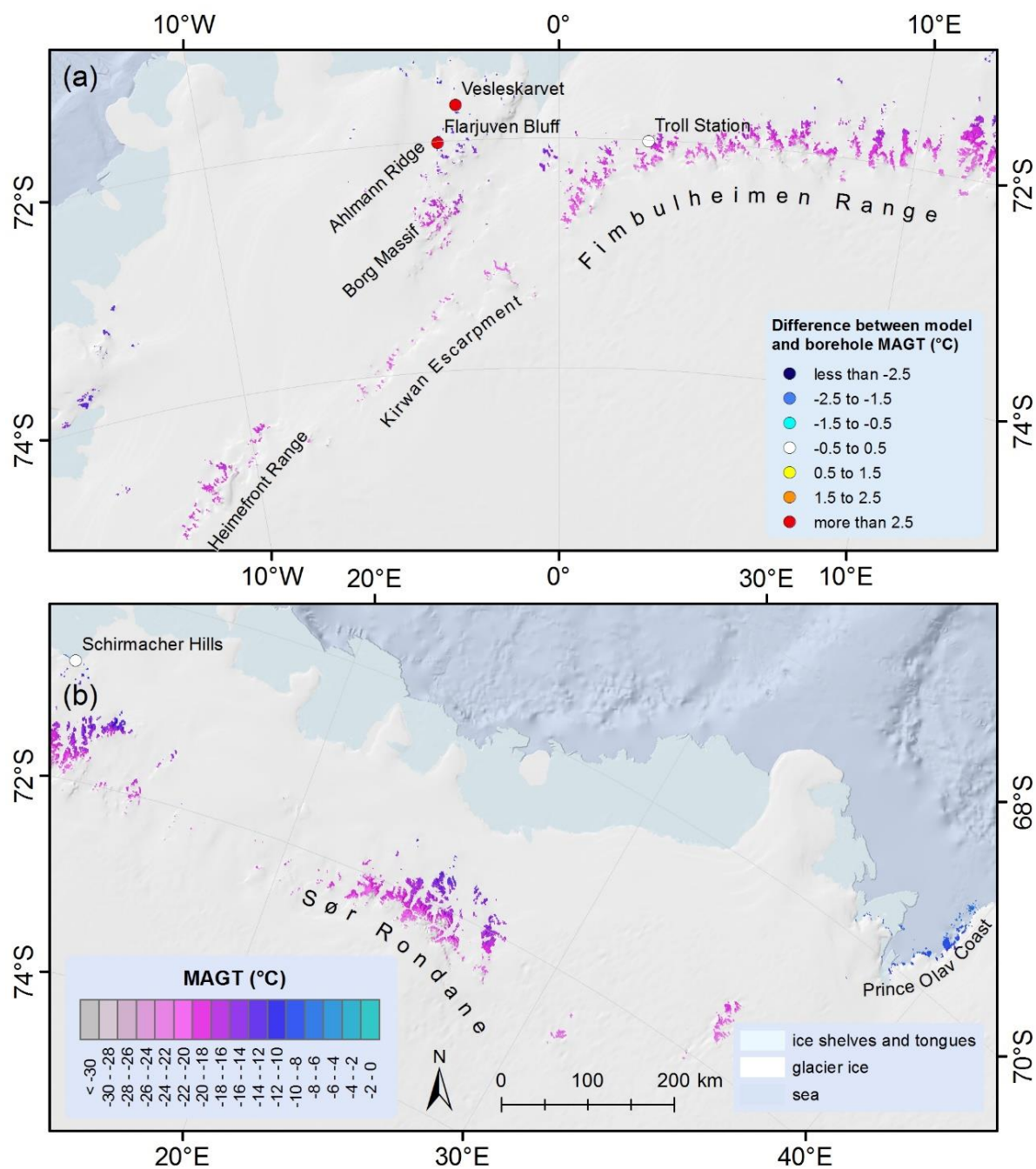


Figure 3: Permafrost temperature maps of Queen Maud Land and differences between borehole and modelled MAGT. See Fig. 1 for location of panels (a) and (b).



3.3 Enderby Land

Permafrost occupies 1140 km² of ice-free area in Enderby Land, which is predominantly mountain tops and a few coastal sites. The modelled average MAGT was -11.7 °C, ranging from -22.4 °C, on summits exceeding 2000 m elevation, to -6.3 °C in the northwest part of the coast (Fig. 4). The MAGT was modelled as around -8 °C at the majority of the coast and around -10 °C in the coastal areas of the Nye, Scott and Tula Mountains, dropping below -15 °C at elevations exceeding 1000 m a.s.l. In the Framnes Mountains, MAGT was modelled at between -17 and -12 °C.

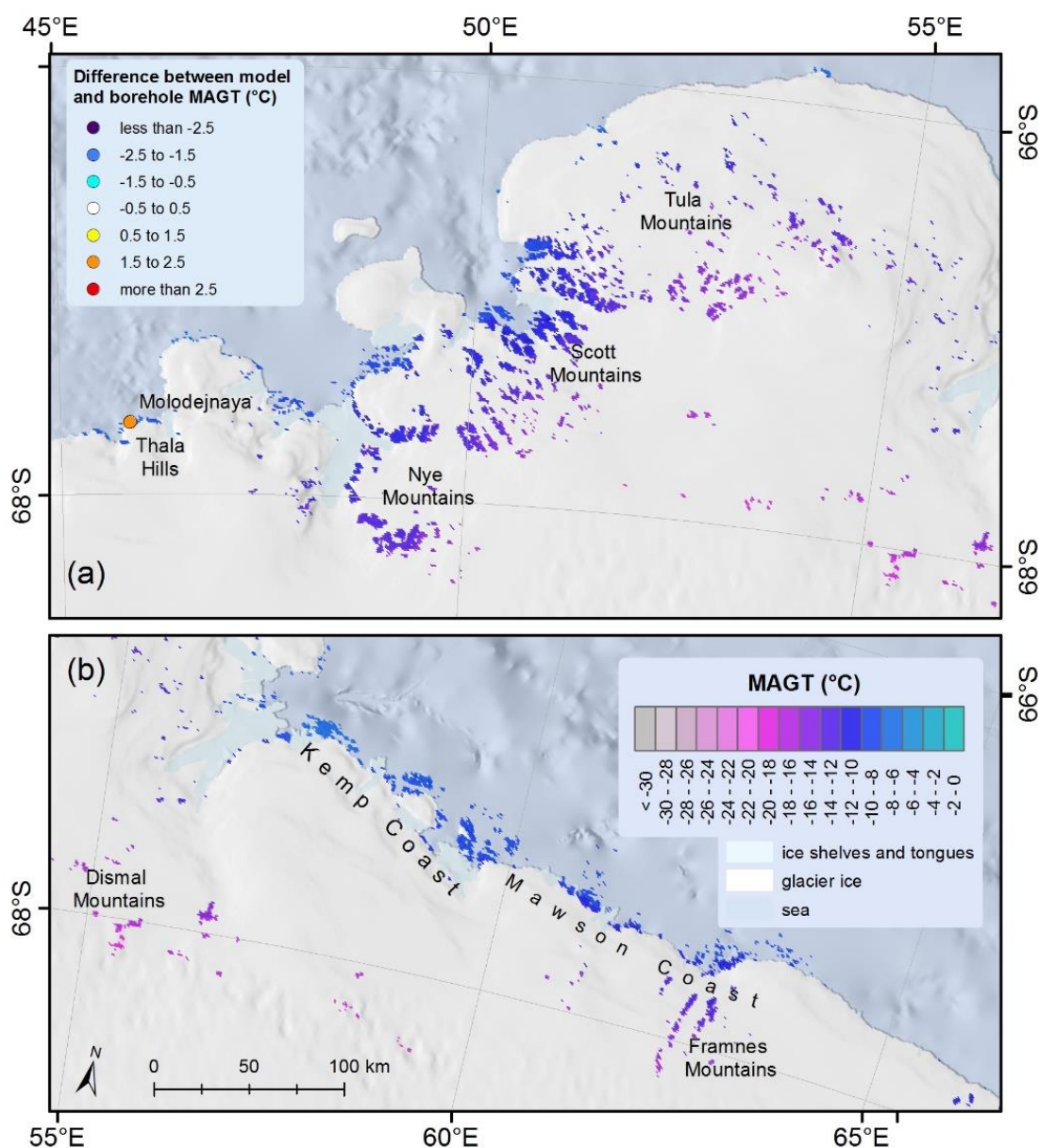




Figure 4: Permafrost temperature maps of Enderby Land and differences between borehole and modelled MAGT. See Fig. 1 for location of panels (a) and (b).

3.4 Vestfold Hills

- 5 The ice-free area of the Vestfold Hills region is 2750 km². The modelling showed an average MAGT of -17.4 °C in this region. The MAGT ranged from -6.6 °C on the islands of the Ingrid Christensen Coast to -28.3 °C in the highest parts of the Prince Charles Mountains (Fig. 5). The MAGT in Amery Oasis, which is a part of the Prince Charles Mountains, was modelled as -13 °C, in the lowest-lying areas, down to -18 °C at elevations approaching 1000 m a.s.l. At the similar elevations on the Mawson Escarpment significantly lower MAGTs, from -19 °C at 200 m a.s.l down to -24 °C at 1500 m a.s.l were recognised.
- 10 In the coastal lowland areas of the Larsemann and Vestfold Hills the MAGT ranged between -10 to -7 °C.

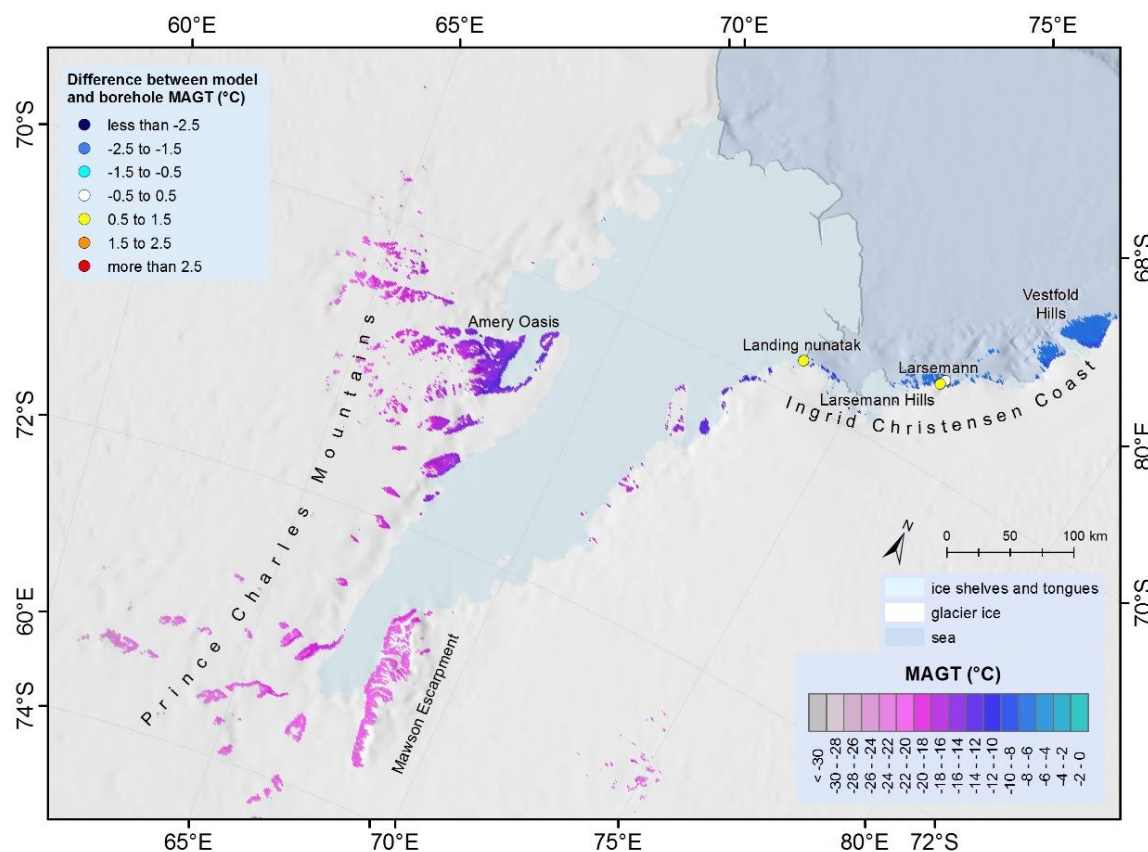
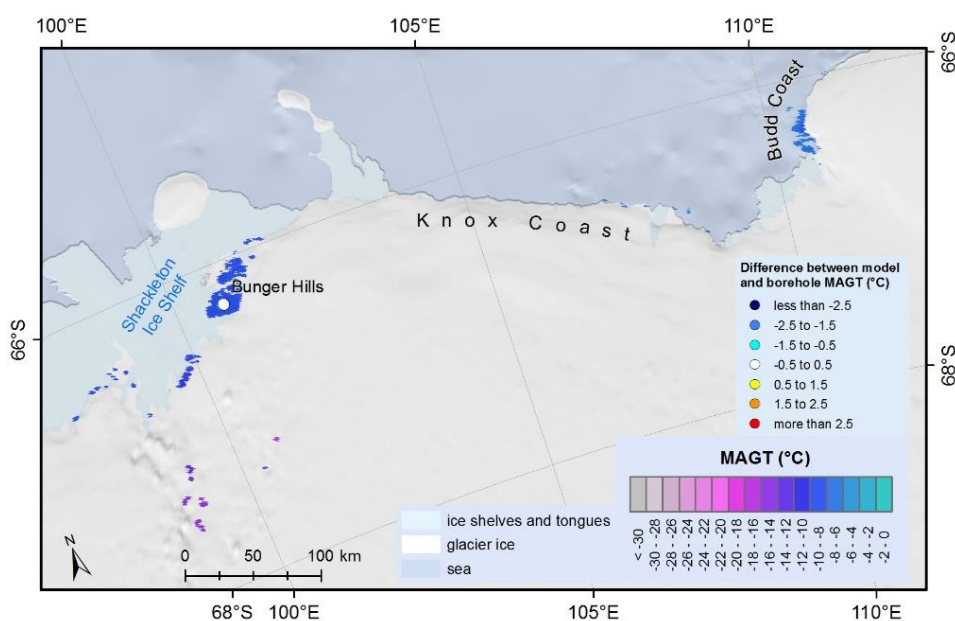


Figure 5: Permafrost temperature map of the Vestfold Hills and differences between borehole and modelled MAGT.



3.5 Wilkes Land

The majority of the 400 km² of ice free area in Wilkes Land lies in the area surrounding the Bunger Hills, where MAGTs of around -9°C were modelled close to the Shackleton Ice Shelf. The lowest MAGT of -15.9 °C was modelled on the adjacent mountains at 1300 m elevation (Fig. 6). Modelled MAGTs were -8 to -6 °C at the Budd Coast, -8 °C at the Adélie Coast, and -10 to -11 °C at the George V Coast. Due to the prevalence of low-lying regions the mean MAGT of the region was only -8.9 °C.



10 **Figure 6: Permafrost temperature maps of Wilkes Land and differences between borehole and modelled MAGT. See Fig. 1 for location.**

3.6 Transantarctic Mountains

The Transantarctic Mountains are the largest ice-free region, comprising 19 750 km² and extending from Cape Adare to Coats Land. The part west of the 90° meridian (Fig. 7) consists of mountain ranges mostly lower than 2000 m (except for the Thiel Mountains) that don't extend to the sea level. The highest MAGT of -17.0 °C was modelled at the foot of the Shackleton Range and the Pensacola Mountains. The MAGTs decreased down to -29 °C in the high mountains. The lowest MAGT of -29.8 °C was modelled in the Thiel Mountains.

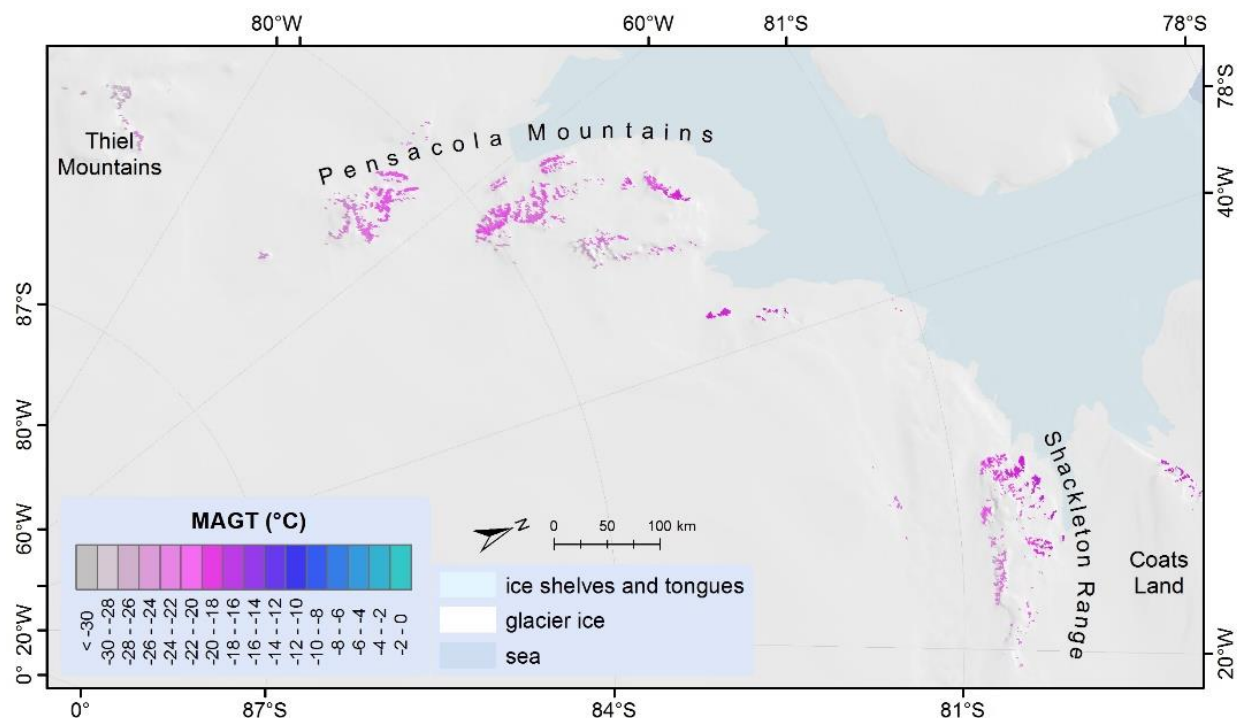


Figure 7: Permafrost temperature map of the Transantarctic Mountains west of the 90° meridian. See Fig. 1 for location.

The region east of the 90° meridian (Fig. 8) consists of numerous mountain ranges extending from the Ross Ice Shelf and Ross Sea up to more than 4000 m elevation and from 85° S to 69° S latitude. The results show the widest range of MAGTs among all the regions with the lowest temperature of -33.5 °C at Mount Markham in Queen Elizabeth Range to -8.5 °C on the Oates Coast. The modelled MAGTs close to the Ross Ice Shelf decreased northwards from -15 °C at the Amundsen Coast to -18 °C at the north of the Dufek Coast. Similar MAGTs, of between -19 and -17 °C were modelled further north along the ice shelf at the Shackleton and Hillary Coasts. Similar decreases in MAGT at higher elevations in the northward direction were observed, but local MAGT variations in relation to altitude were considerable. However, MAGTs below -30 °C were modelled at the highest parts of the mountain ranges along the Ross Ice Shelf. Higher MAGTs were modelled along the Ross Sea and range between -15 °C and -12 °C along the Scott and Borchgrevink Coasts. The modelled MAGTs were around -10 °C at Cape Adare and between -13 and -10 °C on the Pennell Coast. MAGT was modelled down to -26 °C in the Prince Albert Mountains at elevations above 2000 m a.s.l. They approach -30 °C at the highest elevations, that exceed 3000 m a.s.l., in the Deep Freeze Range. Despite the elevations reaching 4000 m a.s.l in the Admiralty Mountains, the MAGT was only down to -23 °C.

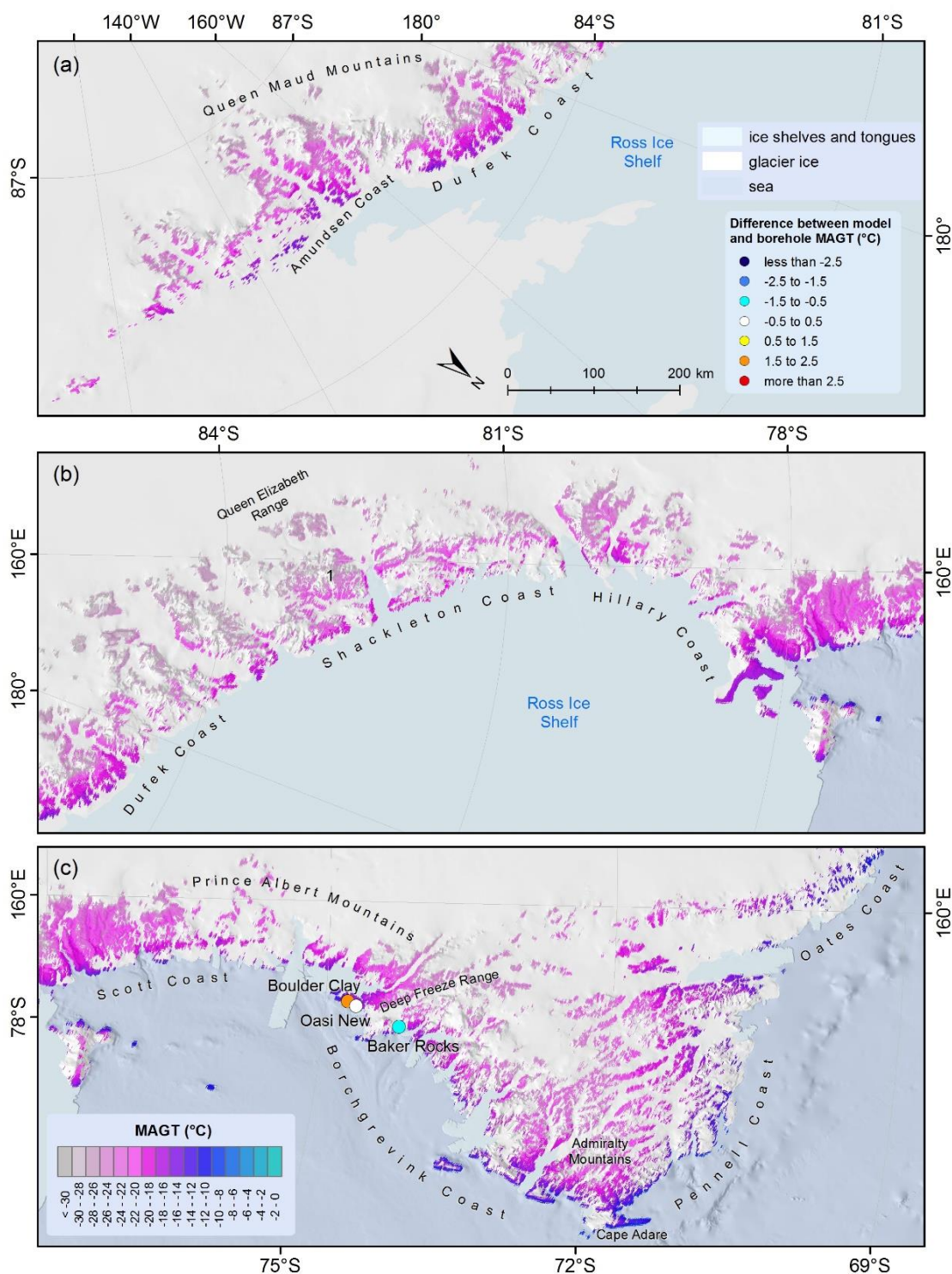


Figure 8: Permafrost temperature maps of the Transantarctic Mountains east of the 90° meridian and differences between borehole and modelled MAGT. See Fig. 1 for location of panels (a), (b) and (c).



3.6.1 McMurdo Dry Valleys

The McMurdo Dry Valleys are a part of Transantarctic Mountains and include a large ice-free area (6700 km²) and are one of the most extensively studied permafrost regions in Antarctica (Bockheim et al., 2007). The lowest MAGT among the dry valleys is modelled in the Victoria Valley falling below -24 °C at the lowest part (Fig. 9). A winter ground temperature inversion is pronounced with MAGTs in the surrounding valleys modelled at around -21 °C. The MAGT also increases up the valleys to -21 °C in the McKelvey, Balham and Barwick Valleys. No MAGT inversion was modelled in the Wright Valley, where MAGTs ranged between -21 and -19 °C and in the Taylor Valley, which is the warmest with MAGT of -17 °C in the lower-lying parts, and -20 °C in the upper part, of the valley. At the Olympus and Asgard Ranges and the Kukri Hills, which surround the valleys, MAGTs of between -23 and -20 °C were modelled. In the surrounding mountains, close to the ice sheet, modelled MAGTs were around -25 °C and reached -27 °C at the highest and the most east-lying mountains. MAGTs at the coast of McMurdo Sound ranged from -13 to -17 °C. On Ross Island, the MAGT was modelled to -16 °C at the Scott and McMurdo Bases which are near sea level and down to -24 °C on Mount Erebus.

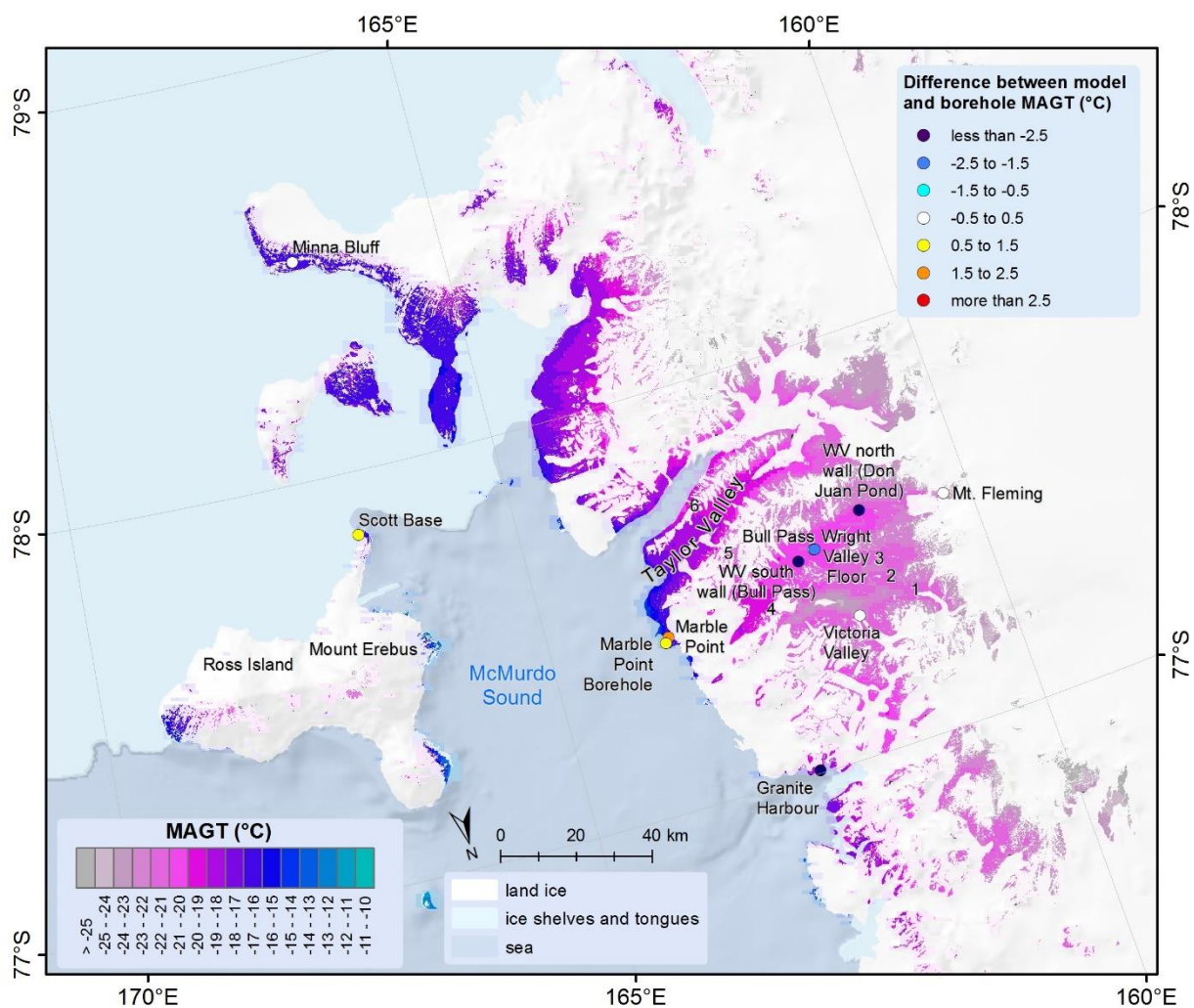


Figure 9: Permafrost temperature map of the McMurdo Dry Valleys and differences between borehole and modelled MAGT. See Fig. 1 for location. Note: the MAGT colour ramp is different from other figures. 1: McKelvey Valley; 2: Balham Valley; 3: Barwick Valley; 4: Olympus Range; 5: Asgard Range 6: Kukri Hills.

5

3.7 Ellsworth Mountains

The ice-free area of the Ellsworth Mountains occupies 380 km² of high-elevation terrain; therefore the modelled mean MAGT was -21.5 °C. The highest temperature was modelled at the foot of the mountains (-17.4 °C) at 500 m a.s.l. with -21 °C at 1000 m a.s.l., -22 °C at 2000 m, and down to -26.1 °C at the highest elevations of Vinson Massif (Fig. 10).

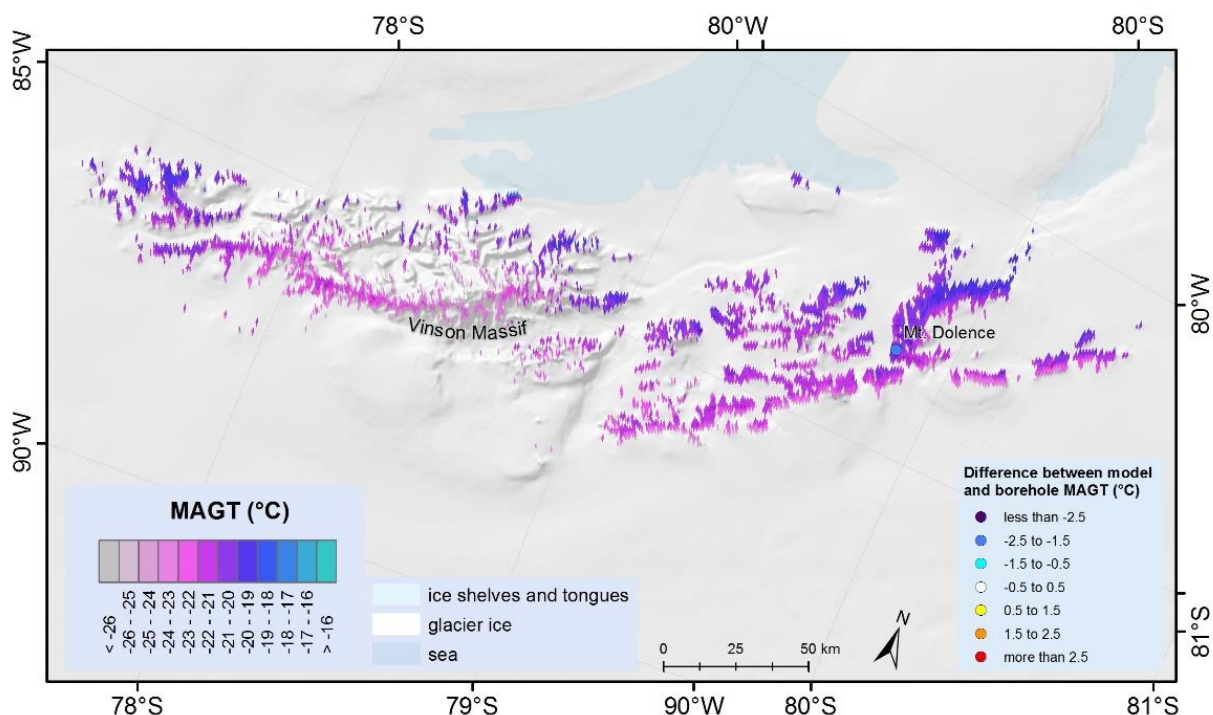


Figure 10: Permafrost temperature map of the Ellsworth Mountains and differences between borehole and modelled MAGT. See Fig. 1 for location.

3.8 Marie Byrd Land

- 5 The ice free areas in Marie Byrd Land occupy only 210 km² and consist mostly of rock outcrops at lower elevations close to the coast and volcanos protruding through the ice sheet. In the Ford Ranges, MAGT was modelled as from -10 °C close to sea level to -16 °C at elevations exceeding 1000 m a.s.l (Fig. 11). MAGTs between -11 and -8 °C were modelled at the Hobbs, Walgreen, Eights and Ruppert Coasts, reaching -6 °C on the islands surrounded by open sea. The volcano-mountain ranges reaching 3000 m a.s.l. (Flood and Kohler Range), had MAGTs typically ranging between -16 to -14 °C at their peaks. Modelled
- 10 MAGTs were between -25 and -21 °C on the Executive Committee Range, where rock outcrops occur above 2000 m a.s.l. and the highest peaks extend to over 4000 m a.s.l.

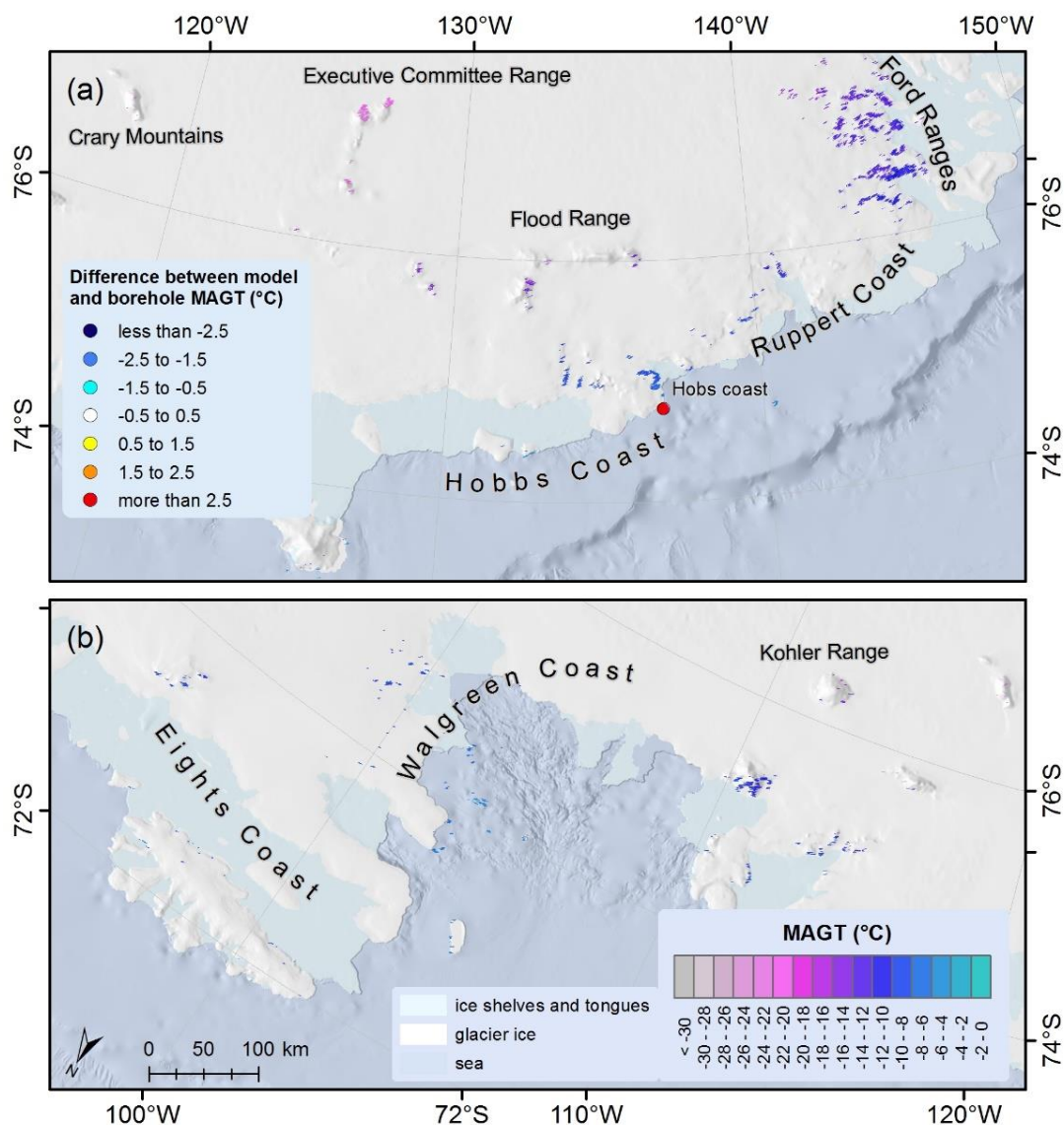


Figure 11: Permafrost temperature maps of Marie Byrd Land and differences between borehole and modelled MAGT. See Fig. 1 for location of panels (a) and (b).

5 3.9 Antarctic Peninsula

The ice-free areas of the Antarctic Peninsula cover 3 800 km² including the South Shetland islands where modelled MAGT was slightly below 0°C and the mountains of the south-eastern Antarctic Peninsula with modelled MAGT of around -19 °C. The modelled near-surface permafrost temperatures in the Antarctic Peninsula were the warmest among all Antarctic regions with an average modelled MAGT of -7.3 °C (Fig. 12).

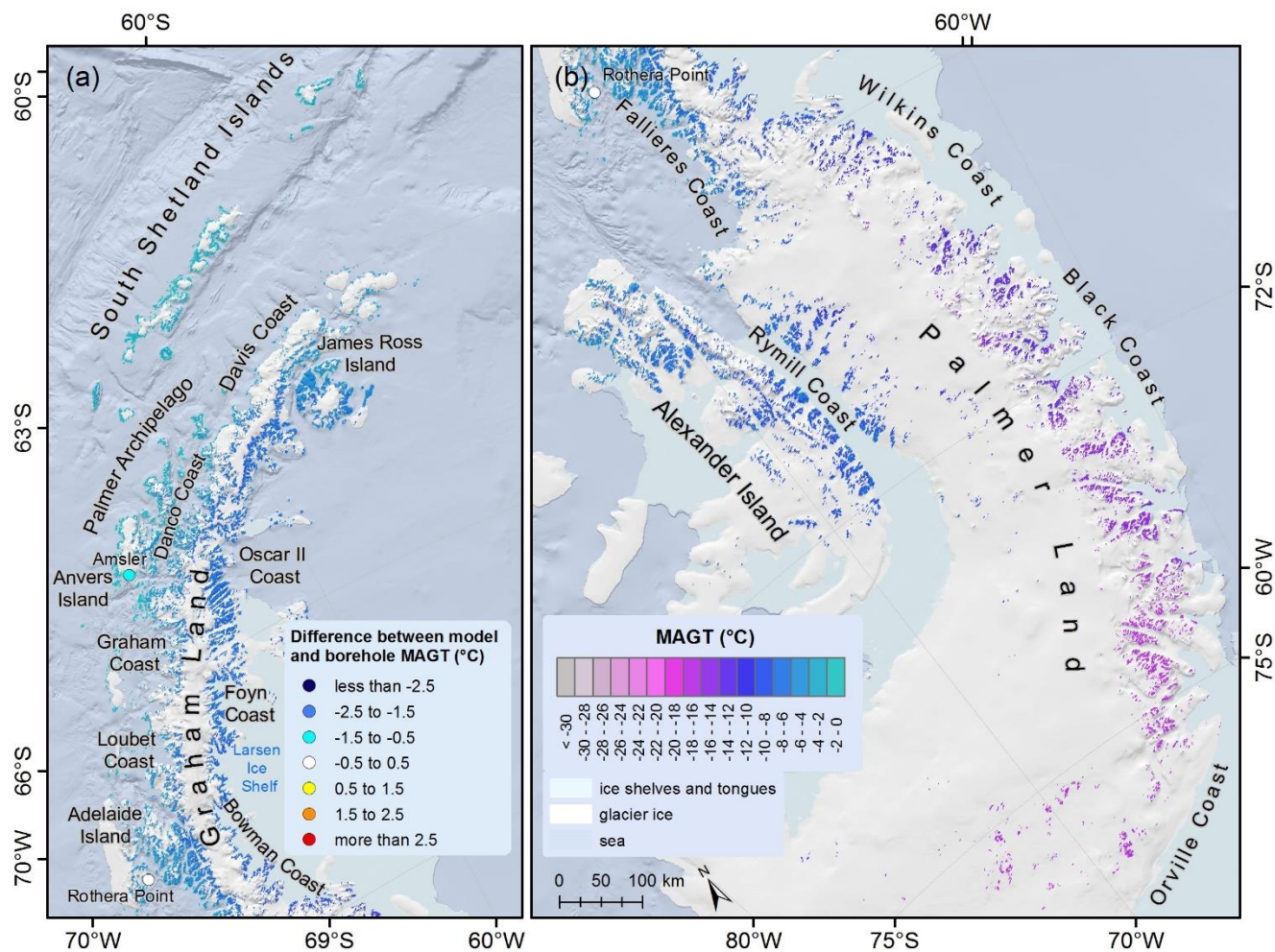


Figure 12: Permafrost temperature maps of the Antarctic Peninsula and differences between borehole and modelled MAGT. See Fig. 1 for location of panels (a) and (b).

5 3.9.1 Palmer Land

The mountains of Palmer Land show considerable differences between the eastern and western parts of the peninsula. Modelled MAGTs at the mountains of the Orville Coast were around $-17\text{ }^{\circ}\text{C}$, increasing to about $-12\text{ to }-15\text{ }^{\circ}\text{C}$ at the Black Coast and eventually rising above $-10\text{ }^{\circ}\text{C}$ at the Wilkins Coast. On the west side at the Fallieres Coast MAGTs of up to $-4\text{ }^{\circ}\text{C}$ were modelled. Temperatures decreased to $-6\text{ to }-8\text{ }^{\circ}\text{C}$ at the Rymill Coast, around $-10\text{ }^{\circ}\text{C}$ at 1000 m a.s.l. , and approached $-12\text{ }^{\circ}\text{C}$ at 1500 m a.s.l. . Similar MAGT ranges were modelled on Alexander Island where MAGTs close to the coast were around $-5\text{ }^{\circ}\text{C}$, decreasing to between $-9\text{ and }-7\text{ }^{\circ}\text{C}$ at 1000 m a.s.l. and falling below $-10\text{ }^{\circ}\text{C}$ at elevations above 2000 m a.s.l.



3.9.2 Graham Land

A considerable increase in modelled MAGT from the east to the west of Graham Land was observed, where the south part of the east coast is protected by the Larsen Ice Shelf. Ground temperatures gradually increased in the northward direction on both sides of the peninsula. MAGTs at the Bowman and Foyn Coasts ranged between -8 and -6 °C and slowly increased from -6 °C at the Oscar II Coast to around -4 °C at the northern-most part of the mainland although still falling below -8 °C at higher elevations. On the west side, MAGT gradually decreased from around -2 °C in the north Davis Coast to -5 °C at the south of the Danco Coast and Anvers Island, where MAGT also fell below -6°C at higher elevations. Similar MAGT ranges were observed at the Graham and Loubet Coasts and at Adelaide Island but were lower than -7 °C at higher elevations. Small Islands along the west coast of the Antarctic Peninsula had a modelled MAGT of between -3 and -1 °C.

10

3.9.3 South Shetland Islands and James Ross Island

Another frequently studied area in the Antarctic is the Northern Antarctic Peninsula, especially the South Shetland Islands. At sites close to sea level, the modelled MAGT was usually above -1 °C on the South Shetland Islands (Fig. 13). MAGT decreased below -2 °C on sites that are not adjacent to the coast but still low-lying such as Byers and Hurd Peninsulas on Livingston Island and Fildes Peninsula on King George Island. The MAGT was below -4 °C on the highest unglaciated peaks of Livingston and Smith Islands and reached -3 °C on Deception Island.

Modelled MAGTs were significantly colder on James Ross Island than on the South Shetland Islands, and, at sites adjacent to the sea, ranging from -3 °C in the north down to -5 °C in the south. Lower lying ice-free areas, including Seymour Island, had MAGTs typically between -6 and -5 °C. The MAGTs on the highest rock outcrops were modelled as down to -7 °C.

20

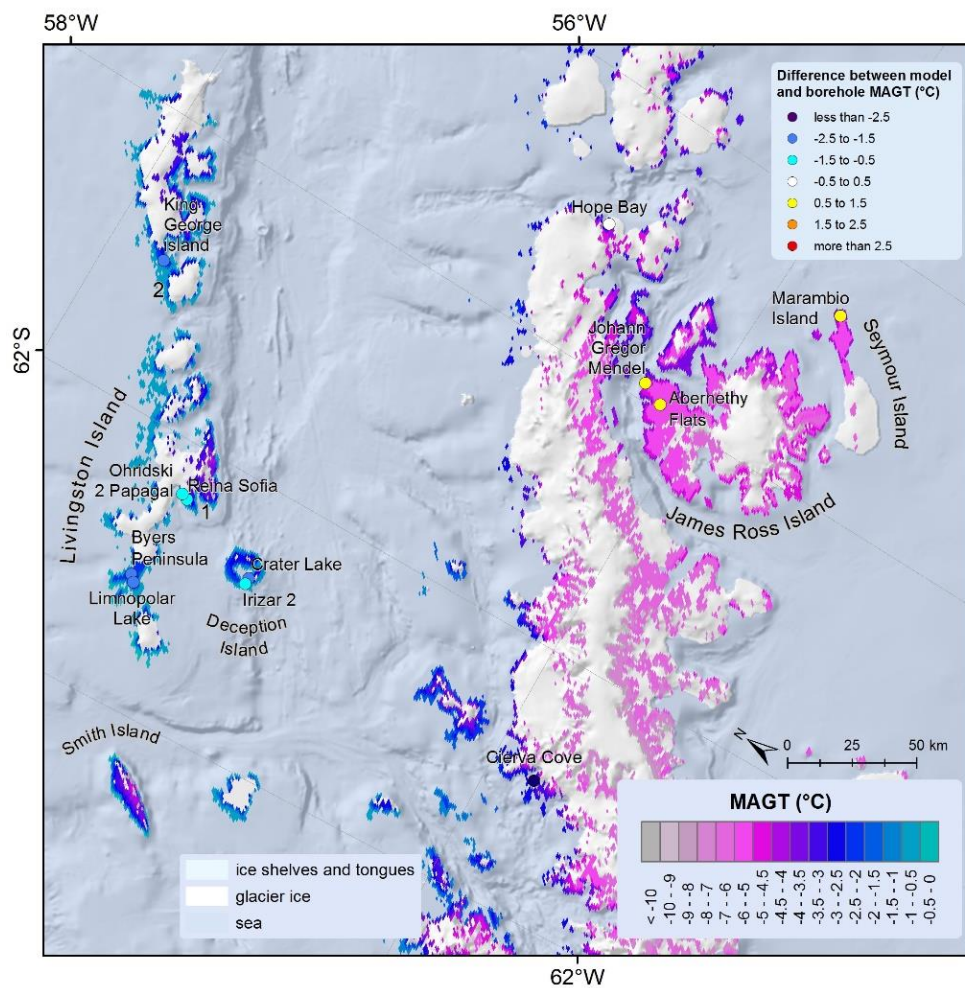


Figure 13: Permafrost temperature map of the Northern Antarctic Peninsula and differences between borehole and modelled MAGT. See Fig. 1 for location. Note: the MAGT colour ramp is different from other figures. 1: Hurd Peninsula; 2: Fildes Peninsula.

3.10 Other Antarctic and sub-Antarctic Islands

5 The modelling results were derived for the Antarctic Islands and sub-Antarctic Islands where the size and ice-free area of the island is sufficient that MODIS LST data were available. MAGT on Signy Island ranged from $-1.5\text{ }^{\circ}\text{C}$ at the coast to $-4\text{ }^{\circ}\text{C}$ in the interior. Permafrost was modelled on all South Sandwich Islands with similar MAGT ranges to those on Signy Island (Fig. 14). Less permafrost is modelled on South Georgia Island, where MAGTs at the coast increase to $1\text{ }^{\circ}\text{C}$ and sporadic permafrost starts to occur at elevations above 100 m. The MAGTs decreased below $-2\text{ }^{\circ}\text{C}$ at the highest-lying rock outcrops. No permafrost

10 was modelled on the Crozet Islands. MAGTs below $0\text{ }^{\circ}\text{C}$ were modelled at the highest elevations of Kerguelen Island and in isolated permafrost patches occurring above 500 m a.s.l. Permafrost is present also on the southern-most ice-free area of Heard Island.

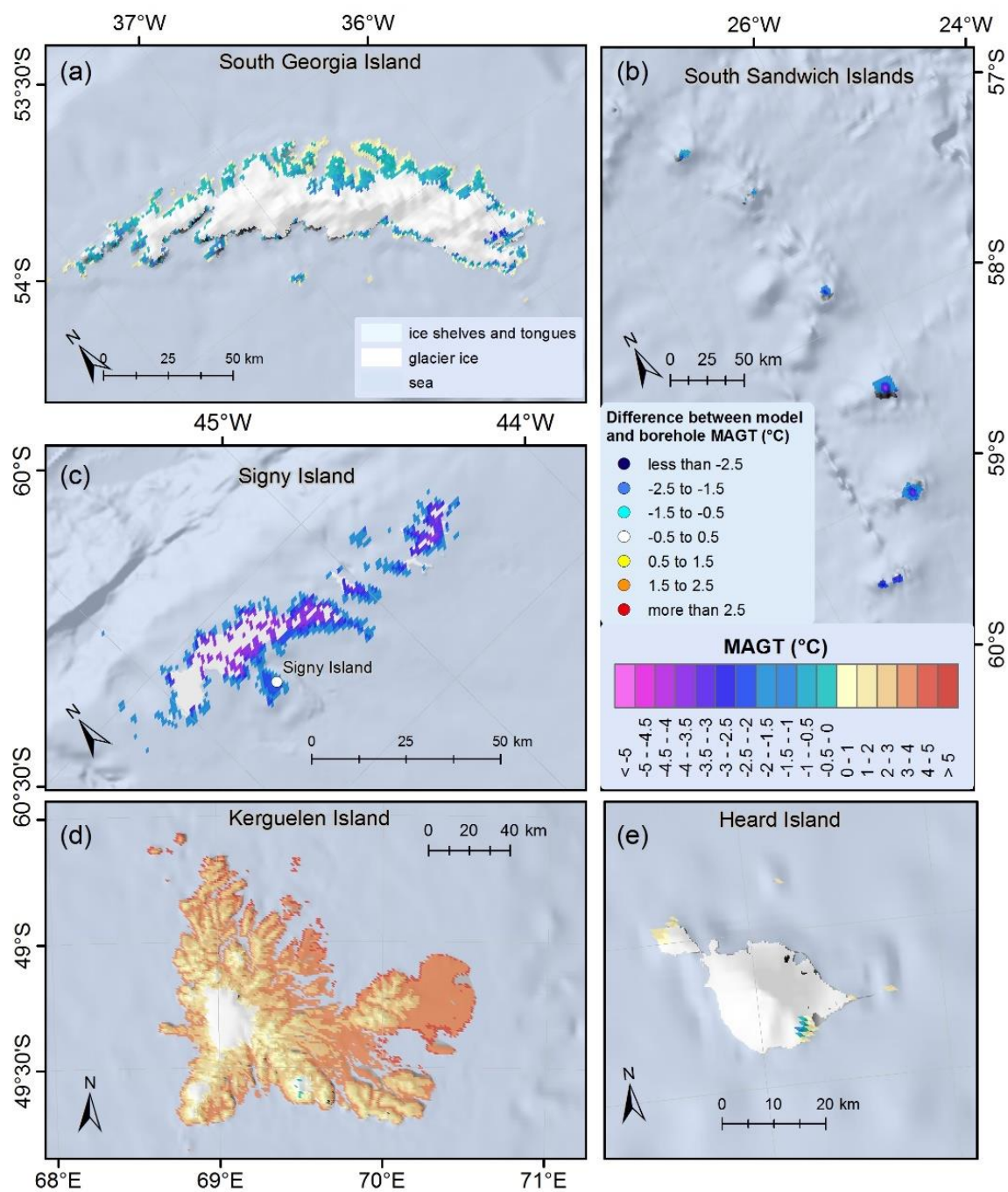


Figure 14: Permafrost temperature maps of Antarctic Islands and difference between borehole and modelled MAGT. See Fig. 1 for location of panels (a), (b), (c), (d) and (e). Note: the MAGT colour ramp is different from other figures.



3.11 Regional MAGT distribution

The MAGT distribution of Antarctic is bimodal with the most pronounced peak at $-21\text{ }^{\circ}\text{C}$ and the second peak at $-7\text{ }^{\circ}\text{C}$ (Fig. 15). The peaks correspond to the two largest ice-free areas of the Transantarctic Mountains and the Antarctic Peninsula, however the temperatures around the $-20\text{ }^{\circ}\text{C}$ peak also occur in other regions such as Queen Maud Land, the Vestfold Hills and the Ellsworth Mountains. The most commonly modelled temperatures were between -23 and $-18\text{ }^{\circ}\text{C}$ and usually occurred in the mountains rising above the Antarctic Ice-sheet and glaciers. MAGTs of between -10 and $-6\text{ }^{\circ}\text{C}$ occurred in the coastal areas of Wilkes Land, Marie Byrd Land, Queen Maud Land, Enderby Land and the Vestfold Hills, but the peak of temperature distribution at coastal sites shifted towards $-7\text{ }^{\circ}\text{C}$ because of MAGTs on the Antarctic Peninsula. The peak of coastal areas would be at $-9\text{ }^{\circ}\text{C}$ if the Antarctic Peninsula was excluded.

10

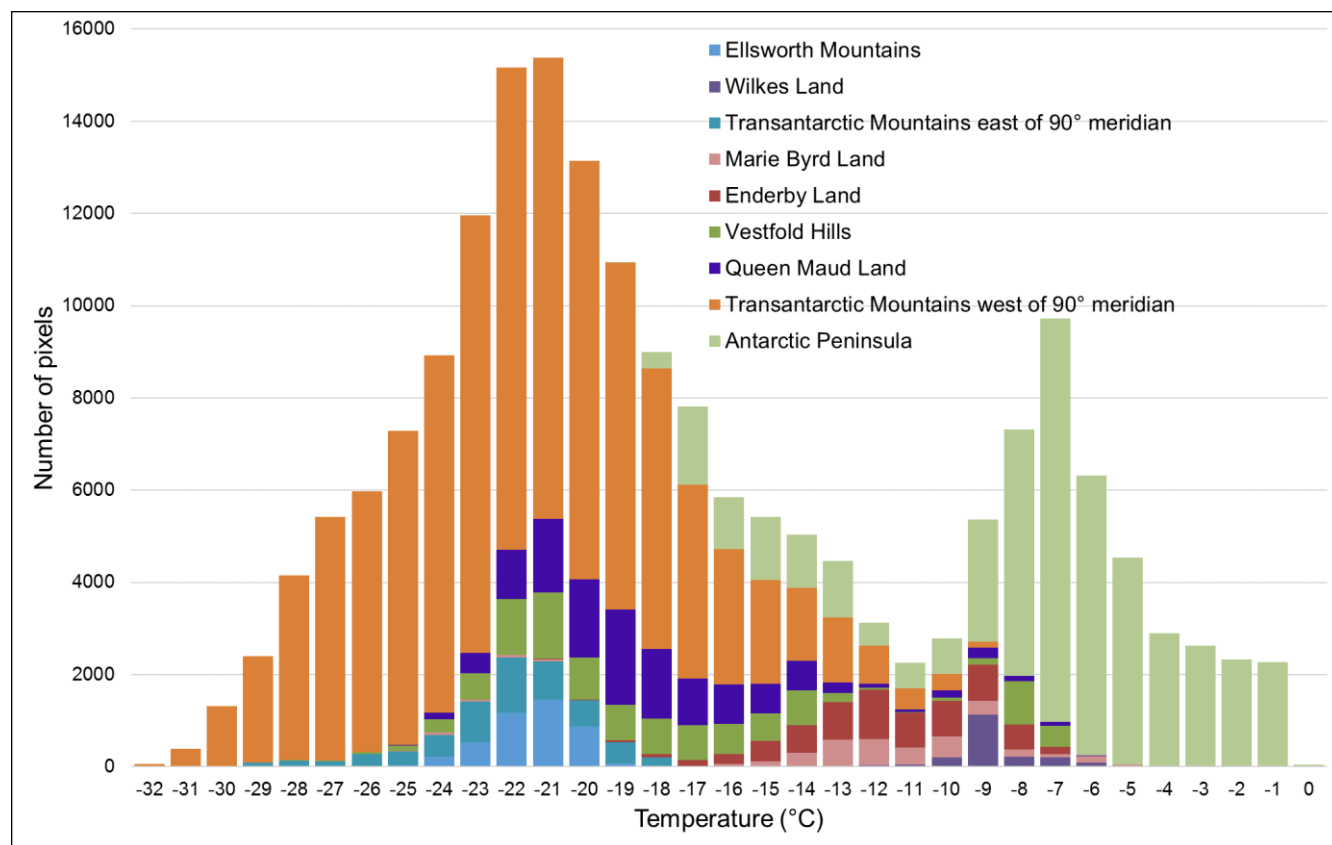


Figure 15: Histogram of temperature distribution across the Antarctic for $1\text{ }^{\circ}\text{C}$ bins. Note: The ice-free areas were often smaller than the analysed pixel size.



3.12 Altitudinal MAGT gradients

Average MAGT lapse rate for the whole Antarctic was $0.40\text{ }^{\circ}\text{C } 100\text{ m}^{-1}$ ranging from $0.15\text{ }^{\circ}\text{C } 100\text{ m}^{-1}$ in the Ellsworth Mountains to $0.59\text{ }^{\circ}\text{C } 100\text{ m}^{-1}$ in Enderby Land. The lapse rates increased from $0.21\text{ }^{\circ}\text{C } 100\text{ m}^{-1}$ in Wilkes Land to $0.38\text{ }^{\circ}\text{C } 100\text{ m}^{-1}$ in the Transantarctic Mountains, $0.44\text{ }^{\circ}\text{C } 100\text{ m}^{-1}$ in the Vestfold Hills, $0.47\text{ }^{\circ}\text{C } 100\text{ m}^{-1}$ in Marie Byrd Land and in
5 the Antarctic Peninsula to $0.49\text{ }^{\circ}\text{C } 100\text{ m}^{-1}$ in Queen Maud Land.

The lapse rates are indicating significant regional differences in the modelled MAGT patterns in relation to elevation (Fig. 16). The warmest among all regions was the Antarctic Peninsula which had MAGTs similar to Marie Byrd Land at around $-12\text{ }^{\circ}\text{C}$ between 1300 m a.s.l., which is again colder at higher elevations. Marie Byrd Land, Queen Maud Land, Enderby Land
10 and Wilkes Land had MAGTs of $-9\text{ }^{\circ}\text{C}$ at the coast but show varying characteristics of temperature decrease with elevation. Marie Byrd Land was the warmest with a decrease in MAGT up to 1500 m a.s.l., and a faster decrease to $-25\text{ }^{\circ}\text{C}$ at 3000 m a.s.l. The slower decrease in temperature with altitude to the 1500m elevation was also modelled in Enderby Land but the MAGT was colder. The MAGT decreased rapidly to $-13\text{ }^{\circ}\text{C}$ at 700 m a.s.l. in Queen Maud Land, where it slightly increased with elevation and then dropped steadily to $-22\text{ }^{\circ}\text{C}$ at 2800 m a.s.l.

15

The modelled MAGT in the Vestfold Hills dropped rapidly from $-10\text{ }^{\circ}\text{C}$ at the coast to $-17\text{ }^{\circ}\text{C}$ at 200 m a. s. l. and then gradually decreased to $-24\text{ }^{\circ}\text{C}$ at 2000 m a.s.l. There are no rock outcrops close to sea level in the Ellsworth Mountains and the MAGT at 100 m a.s.l. was $-20\text{ }^{\circ}\text{C}$. In the Ellsworth Mountains there was a slow decrease of the modelled MAGT, to $-25\text{ }^{\circ}\text{C}$ at 3000 m a. s. l. The coldest MAGTs (below $-30\text{ }^{\circ}\text{C}$) were modelled in the Transantarctic Mountains. In the part west of the 90° meridian,
20 the MAGT dropped from $-20\text{ }^{\circ}\text{C}$ at 500 m a.s.l to $-27\text{ }^{\circ}\text{C}$ at 2000 m a.s.l. but the absolute temperatures were lower east of the 90° meridian where elevations exceed 4000 m a.s.l.

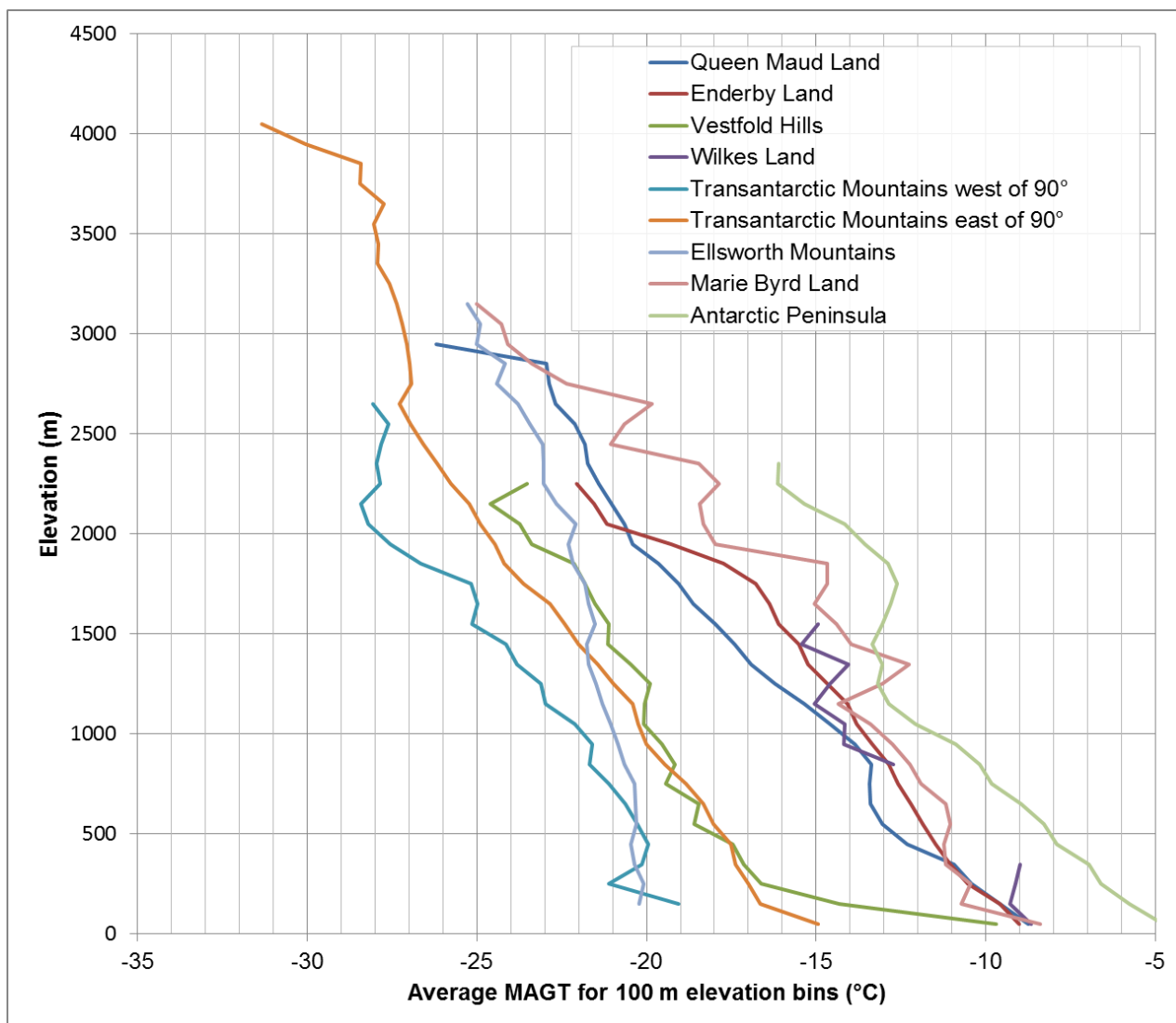


Figure 16: Altitudinal MAGT gradients for Antarctic Soil Regions calculated for 100 m elevation bins.

According to the gradients for sub-regions of the Northern Antarctic Peninsula, the warmest were the South Shetland Islands followed by Palmer Archipelago (Fig. 17). The altitudinal MAGT profiles showed clear differences between the western and eastern parts of the Northern Antarctic Peninsula mainland, although James Ross Island had a similar altitudinal profile to the West Antarctic Peninsula mainland. A significant decrease in MAGT from sea level to 100 m elevation was observed on the South Shetland Islands, Palmer Archipelago and the West Antarctic Peninsula mainland.

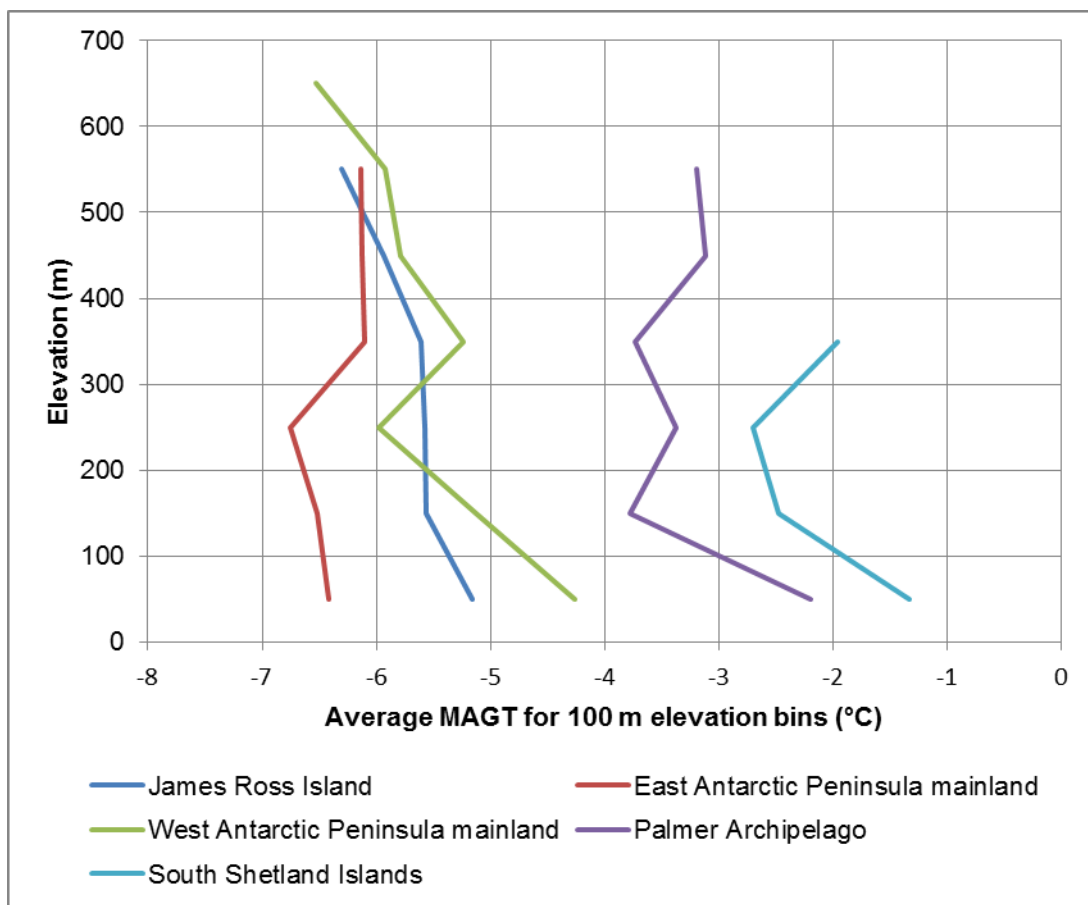


Figure 17: Altitudinal MAGT gradients for the Northern Antarctic Peninsula calculated for 100 m elevation bins.

4 Discussion

5 4.1 Comparison to borehole measurements

4.1.1 Queen Maud Land

The modelled MAGT is according to validation data, was over-estimated in Queen Maud Land. Over-estimation in Schirmacher Hills and Troll Station was below 1 °C but was higher than 4 °C in Flarjuven Bluff and Vesleskarvet. Both stations are located on nunataks, which are exposed to wind that blows away the snow. The estimated 120 mm of annual snowfall resulted in too low n_f -factors for snow-free conditions. However, the minimum MAGT of the ensemble spread approaches the measured MAGT at both stations (Appendix A).



4.1.2 Enderby Land, Vestfold Hills and Wilkes Land

The borehole data in Enderby Land were from the Molodejnaya station (Thala Hills), where modelled MAGT was over-estimated by 1.6 °C. The over-estimation can be explained by rather thin snow cover due to strong winds and snow redistribution at the borehole site, which is confirmed by small differences between measured winter air and ground surface temperatures. The MAGT is accurately modelled in the coastal parts of the Vestfold Hills region, where validation data are available. The difference between modelled and measured MAGT is small at the Larsemann Hills borehole but slight MAGT over-estimation (between 0.6 and 0.9 °C) was observed in comparison to the Larsemann and Landing Nunatak borehole measurements. Similarly, the MAGT was accurately modelled at the Bunger Hills station in the Wilkes Land region, with only small differences in comparison to measured ground temperature.

10

4.1.3 Transantarctic Mountains

The majority of the validation data in the Transantarctic Mountains region is available in the vicinity of the McMurdo Dry Valleys. The sites on the floors of the McMurdo Dry Valleys (Victoria Valley, Wright Valley Floor and Bull Pass) were modelled well with slight over-estimation in Victoria Valley and under-estimation of around 1 °C in the Wright Valley. Two observation sites on small terraces on the walls of the Wright Valley (WV south wall and WV north wall) were modelled 3–4 °C too cold. The difference can be explained by the micro-location of the both sites, which are sheltered from katabatic winds, are above the winter inversion layer, and receive abundant summer solar radiation. The MAGT was over-estimated by up to 1 °C at Mt. Fleming, Scott Base and the Marble Point Borehole, which lie outside the valleys. The MAGT at the Marble Point site, characterised by glacial till, was over-estimated by 2.2 °C, however, the Marble Point Borehole, which was drilled in granite bedrock approx. 1 km away, showed smaller over-estimation. The MAGT was under-estimated by more than 4 °C at the Granite Harbour site which has a warm microclimate as it is situated on north-facing moraine that receives a lot of meltwater from up-slope.

20

Outside the McMurdo Dry Valleys, MAGT measurements from the Zucchelli Station and Baker Rocks are available. The MAGT is over-estimated by 2.3 °C at the Boulder clay borehole, which was drilled in a glacial till, exposed to katabatic winds, and characterised by numerous snow drifts (Guglielmin, 2006) which causes high local variability in permafrost conditions. On the other hand, the MAGT was over-estimated by only 0.2 °C at the Oasi New borehole, which is located in a granitic outcrop. MAGT at the Baker Rocks site, which is situated in littoral deposits (Raffi and Stenni, 2011), was under-estimated by 0.9 °C.

25



4.1.4 Marie Byrd Land

The only available borehole data in Marie Byrd Land is from the Russian research station Russkaya (the name of the borehole is Hobbs coast). According to the measured MAGT between 2008–2013 the modelled MAGT is over-estimated by 3.4 °C. The area is characterised by frequent storms and very strong winds, which blow off most of the snow on one hand and decrease the number and quality of the MODIS measurements on the other hand. The snow free-conditions at the Hobbs coast borehole site were likely not simulated by the snow model, which resulted in the MAGT over-estimation. An alternative explanation could be the measurement period, which is only five years in comparison to 17 modelled years. No validation data were available for the higher elevations of the volcanic ranges. The modelled MAGTs there might be under-estimated because the TTOP model doesn't account for the ground heat flux. This can especially be the case in the locations with recent volcanic activity.

4.1.5 Antarctic Peninsula

Comparison of the modelled MAGT with measured MAGT in boreholes showed an under-estimation in the Western Antarctic Peninsula and slight over-estimation in the Eastern Antarctic Peninsula. The MAGTs are under-estimated by between 1 and 2.1 °C on the South Shetland Islands (King George, Livingston and Deception Island). These under-estimations may be explained by heat advection from meltwater and rain that is not simulated by the model but is especially common in this part of the Antarctic. Another possible explanation for deviations of the modelled MAGT in the north-eastern Antarctic Peninsula are the frequent cloudy conditions. Although clouds are generally masked out from the MODIS LST and replaced by ERA Reanalysis temperatures, measurements in some areas are still contaminated with cloud temperatures, which results in MAGT under-estimation (Østby et al., 2014).

Recent shallowing of thaw depth and ground cooling were observed on Deception Island by Ramos et al. (2017). However, similar cooling was recorded also in the Eastern Antarctic Peninsula, but MAGT was over-estimated by 1.4 °C at Marambio Island and by 0.8 °C at Abernethy Flats and 0.6 °C at the Johann Gregor Mendel borehole sites. MAGT was over-estimated by only 0.2 °C at the Hope Bay mainland site which suggests that there was a continuous gradient of MAGT over-estimation from the Eastern Antarctic Peninsula to MAGT under-estimation on the Western Antarctic Peninsula.

4.2 Permafrost controls

The modelled permafrost temperatures reflect the climatic characteristics of the Antarctic with major controls of latitude, elevation and continentality (Vieira et al., 2010). The effects of the ocean and continentality are well reflected in altitudinal MAGT profiles in Figs 16 and 17. Regions with areas close to the open sea generally show faster MAGT decrease with



elevation, which was observed especially in the Vestfold Hills, the Transantarctic Mountains east of 90° meridian and in Marie Byrd Land where the MAGT dropped significantly with the first elevation increase of 100 or 200 m. The same phenomenon was observed in the North Antarctic Peninsula on the South Shetland Islands, Palmer Archipelago and on the West Antarctic Peninsula mainland where there is less sea ice presence in comparison to James Ross Island and the West Antarctic Peninsula mainland where this MAGT decrease was not observed. The continental mountainous regions of the Ellsworth Mountains and the Transantarctic Mountains west of the 90° meridian have, on the other hand, no open sea in the vicinity and had a significantly slower MAGT drop with the altitude.

The modelled MAGT lapse rate of 0.40 °C 100 m⁻¹ for the whole Antarctic is lower than the average air temperature lapse rate of 0.65 °C 100 m⁻¹ in the International Standard Atmosphere (ISO 2533:1975) but is, however, the same as the mean air temperature lapse rate measured for ice-free sites on James Ross Island from 2013–2016 (Ambrozova et al., 2019). Small increases of MAGTs with elevation were observed in many regions. This might be attributed to the nature of the analysis rather than a presence of temperature inversions. The rock outcrops on the scale of the regions are often present at different elevations far from each other, which results in occurrence of higher MAGTs at higher elevations. Additionally, some elevation bins have only a few rock outcrop pixels, which makes the averaged MAGT less representative for the whole region.

The lowest MAGT of -33.5 °C was modelled in the Transantarctic Mountains at the Queen Elizabeth Range, where the highest peak reaches 4350 m. The MAGT there could fall below -36 °C according to the coldest ensemble member. This is the lowest MAGT modelled on Earth according to the modelling in the other parts of the globe (Obu et al., 2019). On the highest Antarctic peak Mount Vinson in the Ellsworth Mountains reaching 4892 m a MAGT of only -26.1 °C was modelled. The Queen Elizabeth Range lies approximately 5° further south than Mount Vinson, illustrating the effect of latitude on permafrost temperatures.

The winter air temperature inversions that occur in the McMurdo Dry Valleys result in air temperatures that are approx. 10 °C lower in the valleys than in the surroundings, but inversions are occasionally disrupted by katabatic winds from the polar ice sheet (Nylen et al., 2004). The winter inversions reflect in MAGTs being approx. 3 °C colder on the floor than in surroundings in Victoria Valley, where the inversions are particularly intense in comparison to other valleys. No MAGT inversions were modelled in the Wright Valley, which lies only 50 m a.s.l (though winter temperature inversions do occur there), or in the Taylor Valley, which is opened to the coast and can drain cold air.

4.3 Model performance and limitations

As the LST data are primarily derived from satellite data, their availability and accuracy depend on cloud cover. On one hand the frequent cloud cover might be a reason for general under-estimation of modelled MAGT at Antarctic Peninsula. On the



other hand the clear sky conditions in the McMurdo Dry Valleys might explain the relatively successful modelling results in this area.

The absence of vegetation in the Antarctic results in high snow redistribution by wind and highly spatially variable snow cover, which influences ground temperatures in many parts of Antarctic (Guglielmin et al., 2014; Ramos et al., 2017; Ferreira et al. 2017). Neither snow redistribution nor sublimation are simulated by our snowfall model and the average snow depths could not be estimated and n_f -factors derived as for the Northern Hemisphere by Obu et al. (2019). Although an ensemble of 200 model runs with varying annual snowfall is used, the mean of the ensemble runs does not always represent the borehole site microclimate and ground properties. In the case of wind-exposed nunataks where the snow presence is over-estimated on larger areas, such as Flarjuven Bluff and Vesleskarvet, the MAGTs can be over-estimated up to 4 °C, but the modelled ensemble minimum still approaches the measured MAGT.

Several permafrost and active-layer studies in the Antarctic have noted occurrence of n_f -factors above 1 (Lacelle et al., 2016; Kotzé and Meiklejohn, 2017), which indicates that average air temperatures are higher than ground surface temperatures. The likely explanation could be a presence of snow during the warmer part of the year, which is insulating ground from heat, unlike from cold in the winter. However Kotzé and Meiklejohn (2017) mention also a presence of blocky deposits at the Vesleskarvet site, which could result in ground cooling due to cold air advection. The concept of n_f -factors was introduced for the Northern Hemisphere for snowcover effect during freezing conditions (Smith and Riseborough, 1996), which challenges the derivation of n_f -factors for TTOP modelling on sites with highly temporarily variable snow cover.

Elevation is one of the major permafrost controlling factors in the Antarctic (Vieira et al., 2010). In steep terrain, the model input datasets are less likely to be representative for the micro-locations present within the modelled pixel or the borehole site as for example shown on the boreholes sites on the walls of the Wright Valley. A number of the Antarctic boreholes are situated in mountainous environments, which might explain some of the discrepancies between measured and modelled MAGT. Elevation uncertainties in DEM are inherited by the model and reflected in the estimated average annual snowfall and downscaled ERA reanalysis temperatures. The elevations of some peaks might also not be well represented at the spatial resolution of 1 km, therefore the modelled MAGT might appear warmer than MAGT found on the top a peak.

5 Conclusions

Near-surface permafrost temperatures in the Antarctic were most commonly modelled as between -23 and -18 °C for mountainous areas rising above the Antarctic Ice Sheet. The Earth's lowest permafrost temperature of -33 °C was modelled at Mount Markham in Queen Elizabeth Range in the Transantarctic Mountains. Coastal regions were usually characterised with ground temperatures of between -14 and -8 °C, approaching 0 °C in the coastal areas of the Antarctic Peninsula and rising



above 0°C in the Antarctic Islands. The regional variations in permafrost temperatures can be explained by (1) continentality, which influences permafrost temperatures especially, at elevations of up to 200 m; (2) elevation; and (3) latitude, which explains differences in permafrost temperatures at similar elevations.

- 5 Comparison of modelled temperatures to 40 permafrost boreholes and soil climate stations yielded root mean square error of 1.9 °C but the accuracy varied significantly among borehole sites. The difference was smaller than 1 °C for more than 50 % of the sites, but can exceed 4 °C. The greatest differences between the modelled and measured permafrost temperatures occurred where snow conditions were not successfully represented in the model. These sites are generally exposed to a strong wind-driven redistribution of snow as for example at nunataks in Queen Maud Land, on the Hobs Coast, and in Marie Byrd
- 10 Land. Considerable differences between modelled and measured MAGTs also occurred at sites with microclimate and ground properties that are not representative for the respective modelled 1 km² pixel. Permafrost temperatures on the walls of Wright Valley and in Granite Harbour were under-estimated by up to 4 °C, which can be explained by warm microclimates of the borehole sites compared to surroundings. The model performed well in areas with frequent cloud-free conditions such as the McMurdo Dry Valleys, where even winter air temperature inversions are reflected in the modelled permafrost temperatures.
- 15 Frequent cloudy conditions in the north-western Antarctic Peninsula can to some extent explain the systematic under-estimation of modelled permafrost temperatures in this area.

This study is the first continent-wide modelling of permafrost temperatures for the Antarctic. It reports near-surface permafrost temperatures for remote regions without observations, which is highly valuable for research fields, such as climate change, terrestrial ecology, microbiology or astrobiology. Our study suggests that extended networks of currently sparse borehole temperature measurements and spatially distributed information on snow cover and ground properties are crucial for improving future permafrost modelling results in the Antarctic.

20

Data availability: The data are available for download at: <https://doi.pangaea.de/10.1594/PANGAEA.902576>

25

30



Appendix A: List of borehole properties, measurements and modelled results

Borehole name	Latitude	Longitude	Sensor depth (cm)	Elevation (m)	Measured MAGT (°C)	MAGT calculation period	Modelled mean MAGT (°C)
Johann Gregor Mendel	-63.80000	-57.86670	75	10	-5.60	2011-2017	-4.98
Abernethy Flats	-63.88140	-57.94830	75	n/a	-6.15	2006-2016	-5.38
Bunger Hills	-66.27530	100.76000	500	7	-8.90	2008-2014	-9.09
Schirmacher Hills	-70.77177	11.73673	100	80	-8.50	2009-2016	-8.19
Larsemann Hills	-69.38669	76.37538	500	96	-7.80	2013-2015	-7.83
Larsemann	-69.40421	76.34465	300	96	-8.60	2008, 2010-2015	-7.90
Landing nunatak	-69.74781	73.70503	100	96	-11.00	2011-2012	-10.08
King George island	-62.19667	-58.96556	500	20	-0.70	2008-2009, 2014	-2.21
Hobs coast	-74.76333	-136.79639	50	76	-10.30	2008-2013	-6.86
Molodejnaya	-67.66556	45.84194	50	45	-9.40	2008, 2011-2013, 2015-2016	-7.81
Reina Sofia	-62.67028	-60.38222	n/a	275	-1.78	n/a	-3.05
Cierva Cove	-64.16195	-60.95093	1500	182	-0.95	n/a	-3.67
Amsler	-64.77619	-64.06057	900	67	-0.36	2016-2017	-1.48
Crater Lake	-62.98333	-60.66667	n/a	85	-0.83	n/a	-2.96
Byers Peninsula	-62.62981	-61.06013	n/a	92	-0.43	n/a	-2.33
Limnopolar Lake	-62.64959	-61.10405	130	90	-0.60	2009-2012	-2.34
Rothera Point	-67.57070	-68.11879	n/a	31	-3.10	2009-2011	-2.78
Marambio Island	-64.23333	-56.61667	n/a	200	-6.60	2009-2012	-5.24
Signy Island	-60.71655	-45.59978	n/a	90	-2.10	2006-2009	-2.11
Ohridski 2 Papagal	-62.64811	-60.36375	400	147	-1.04	2008-2018	-1.90
Irizar 2	-62.98263	-60.71562	80	130	-1.58	2009-2017	-2.49
Troll Station	-72.01139	2.53306	3	1275	-17.40	2007-2015	-17.09
Flarjuven Bluff	-72.01167	-3.38833	3	1220	-17.50	2008-2015	-13.06
Vesleskarvet	-71.68998	-2.84758	3	805	-16.10	2009-2014	-11.91
Boulder Clay	-74.74583	164.02139	n/a	205	-16.90	1996-2009	-14.63
Oasi New	-74.70000	164.10000	n/a	80	-13.50	2005-2009	-13.32
Bull Pass	-77.51847	161.86269	60	141	-19.44	2000-2017	-20.93
WV south wall (Bull Pass East)	-77.50219	162.06475	50	832	-16.44	2013-2017	-20.04
WV north wall (Don Juan Pond)	-77.57388	161.23877	50	734	-16.76	2011-2017	-20.83
Granite Harbour	-77.00655	162.52561	66	6	-14.31	2003-2017	-18.53
Marble Point	-77.41955	163.68247	120	47	-18.15	2000-2017	-15.99
Minna Bluff	-78.52500	166.78240	43	32	-16.44	2007-2016	-16.52
Mt. Fleming	-77.54519	160.29027	22	1697	-23.81	2002-2017	-23.58
Scott Base	-77.84831	166.76058	40	44	-17.42	2000-2017	-16.64
Victoria Valley	-77.33178	161.60069	30	410	-22.87	2000-2017	-22.97
Wright Valley Floor	-77.51808	161.85117	75	n/a	-19.13	2000-2017	-20.93
Marble Point Borehole	-77.40732	163.72913	200	85	-16.90	2009-2015	-15.96
Baker Rocks	-74.20750	164.83361	3	11	-15.60	2006-2015	-16.52
Mt. Dolence	-79.82181	-83.19714	30	886	-18.30	2012-2013	-20.21
Hope Bay	-63.40635	-56.99656	80	n/a	-4.10	2010	-3.83



Appendix A: (Continuation)

Borehole name	Difference between Modelled Modelled				Source	Soil Region
	modelled and measured MAGT (°C)	max MAGT	min MAGT	Modelled SD (°C)		
Johann Gregor Mendel	0.62	-2.83	-6.43	0.89	Hrbáček et al., 2017a	Antarctic Peninsula
Abernethy Flats	0.77	-2.89	-6.89	1.08	Hrbáček et al., 2017b	Antarctic Peninsula
Bunger Hills	-0.19	-4.41	-11.50	1.41	Andrey Abramov	Wilkes Land
Schirmacher Hills	0.31	-3.91	-9.95	1.08	Andrey Abramov	Queen Maud Land
Larsemann Hills	-0.03	-3.53	-9.82	1.23	Andrey Abramov	Vestfold Hills
Larsemann	0.70	-3.64	-9.76	1.17	Andrey Abramov	Vestfold Hills
Landing nunatak	0.93	-6.10	-12.39	1.33	Andrey Abramov	Vestfold Hills
King George island	-1.51	-0.93	-2.75	0.47	Andrey Abramov	Antarctic Peninsula
Hobs coast	3.44	-4.06	-10.14	1.66	Andrey Abramov	Marie Byrd Land
Molodejnaya	1.59	-4.06	-10.19	1.66	Andrey Abramov	Enderby Land
Reina Sofia	-1.27	-1.54	-3.97	0.67	Miguel Ramos	Antarctic Peninsula
Cierva Cove	-2.72	-1.95	-5.51	0.86	Gonçalo Vieira	Antarctic Peninsula
Amsler	-1.12	-0.65	-2.42	0.49	Gonçalo Vieira	Antarctic Peninsula
Crater Lake	-2.13	-1.51	-4.01	0.65	Gonçalo Vieira	Antarctic Peninsula
Byers Peninsula	-1.90	-1.10	-2.95	0.50	Oliva et al. (2017)	Antarctic Peninsula
Limnopolar Lake	-1.74	-1.04	-2.90	0.47	de Pablo et al. (2014)	Antarctic Peninsula
Rothera Point	0.32	-1.36	-3.95	0.74	Guglielmin et al. (2014)	Antarctic Peninsula
Marambio Island	1.36	-3.01	-6.58	0.83	Jorge Strelin	Antarctic Peninsula
Signy Island	-0.01	-0.97	-2.86	0.45	Guglielmin et al. (2012)	Antarctic Islands
Ohridski 2 Papagal	-0.87	-0.93	-2.80	0.43	Gonçalo Vieira	Antarctic Peninsula
Irizar 2	-0.91	-1.21	-3.33	0.60	Gonçalo Vieira	Antarctic Peninsula
Troll Station	0.31	-9.41	-19.56	1.19	Hrbáček et al. (2018)	Queen Maud Land
Flarjuven Bluff	4.45	-6.46	-16.84	2.68	Hrbáček et al. (2018)	Queen Maud Land
Vesleskarvet	4.19	-6.01	-15.09	2.57	Hrbáček et al. (2018)	Queen Maud Land
Boulder Clay	2.27	-8.83	-16.78	1.22	Vieira et al. (2010)	Transantarctic Mountains
Oasi New	0.18	-8.24	-15.08	0.84	Vieira et al. (2010)	Transantarctic Mountains
Bull Pass	-1.49	-17.24	-22.65	0.95	USDA (Seybold et al., 2009)	Transantarctic Mountains
WV south wall (Bull Pass East)	-3.60	-17.35	-21.64	0.90	Megan Balks	Transantarctic Mountains
WV north wall (Don Juan Pond)	-4.07	-18.33	-22.50	0.82	Megan Balks	Transantarctic Mountains
Granite Harbour	-4.22	-15.52	-20.15	0.84	USDA (Seybold et al., 2009)	Transantarctic Mountains
Marble Point	2.16	-13.67	-17.83	0.65	Megan Balks	Transantarctic Mountains
Minna Bluff	-0.07	-10.74	-19.03	1.35	Megan Balks	Transantarctic Mountains
Mt. Fleming	0.23	-19.36	-25.66	1.01	Megan Balks	Transantarctic Mountains
Scott Base	0.78	-10.72	-18.84	1.08	Megan Balks	Transantarctic Mountains
Victoria Valley	-0.10	-21.26	-24.59	0.90	Megan Balks	Transantarctic Mountains
Wright Valley Floor	-1.79	-17.24	-22.65	0.95	Megan Balks	Transantarctic Mountains
Marble Point Borehole	0.95	-11.46	-17.72	0.83	Guglielmin et al. (2011)	Transantarctic Mountains
Baker Rocks	-0.92	-7.11	-19.39	1.59	Hrbáček et al. (2018)	Transantarctic Mountains
Mt. Dolence	-1.91	-13.48	-22.37	1.13	Schaefer et al. (2017b)	Ellsworth Mountains
Hope Bay	0.27	-1.82	-4.97	0.66	Schaefer et al. (2017a)	Antarctic Peninsula



Author contribution: JO, SW, GV, AB and AK designed conceptual framework for the study and the model was developed and ran by SW and JO. Ground validation data was contributed by GV, AA, MB, FH and MR, who also provided interpretation of results on regional scale. JO wrote the paper based from input and feedback from all co-authors.

5

Competing interests: The authors declare that they have no conflict of interest.

Acknowledgements: This work was funded by the European Space Agency Data User Element GlobPermafrost project in cooperation with ZAMG (grant number 4000116196/15/I-NB) and the Research Council of Norway SatPerm project (grant number 239918). Data storage resources were provided by Norwegian National Infrastructure for Research Data (project NS9079K). The work of FH was supported by the Ministry of Education Youth and Sports of Czech Republic large infrastructure project LM2015078. Temperature data for Russian stations were obtained with the support form the Russian Antarctic Expedition and Government program AAAA-A18-118013190181-6. The PERMANTAR observatories in Western Antarctic Peninsula have been funded mainly by the Portuguese Foundation for Science and Technology and the Portuguese Polar Program. The Terra and AQUA MODIS LST datasets were acquired from the Level-1 and Atmosphere Archive & Distribution System (LAADS) Distributed Active Archive Center (DAAC), located in the Goddard Space Flight Center in Greenbelt, Maryland (<https://ladsweb.nascom.nasa.gov/>). Over the years many people have contributed to installation and maintenance of the McMurdo Dry Valley Soil Climate stations, but particular thanks are due to Cathy Seybold, Ron Paetzold and Don Huffman from USDA, Jackie Aislabie and Fraser Morgan, Landcare Research, N.Z., and Chris Morcom, Dean Sandwell, and Annette Carshalton, University of Waikato, NZ. Antarctica New Zealand provided logistic support for annual station access. Authors thank also to Nikita Demidov, Andrey Dolgikh, Elya Zazovskaya, Nikolay Osokin, Dima Fedorov-Davidov, Andrey Ivashchenko, Alexey Lupachev and Nikita Mergelov for borehole data retrieval from the Russian Antarctic Stations.

25

30



References

- Ambrozova, K., Laska, K., Hrbacek, F., Kavan, J. and Ondruch, J.: Air temperature and lapse rate variation in the ice-free and glaciated areas of northern James Ross Island, Antarctic Peninsula, during 2013–2016, *International Journal of Climatology*, 39(2), 643–657, doi:10.1002/joc.5832, 2019.
- 5 Beer, C.: Permafrost Sub-grid Heterogeneity of Soil Properties Key for 3-D Soil Processes and Future Climate Projections, *Front. Earth Sci.*, 4, doi:10.3389/feart.2016.00081, 2016.
- Bintanja, R. and Reijmer, C. H.: A simple parameterization for snowdrift sublimation over Antarctic snow surfaces, *Journal of Geophysical Research: Atmospheres*, 106(D23), 31739–31748, doi:10.1029/2000JD000107, 2001.
- Bockheim, J., Vieira, G., Ramos, M., López-Martínez, J., Serrano, E., Guglielmin, M., Wilhelm, K. and Nieuwendam, A.:
10 Climate warming and permafrost dynamics in the Antarctic Peninsula region, *Global and Planetary Change*, 100, 215–223, doi:10.1016/j.gloplacha.2012.10.018, 2013.
- Bockheim, J. G., Campbell, I. B. and McLeod, M.: Permafrost distribution and active-layer depths in the McMurdo Dry Valleys, Antarctica, *Permafrost and Periglacial Processes*, 18(3), 217–227, doi:10.1002/ppp.588, 2007.
- Bockheim, J. G., Campbell, I. B., Guglielmin, M. and López-Martínez, J.: Distribution of permafrost types and buried ice in icefree areas of Antarctica, in 9th International Conference on Permafrost, Proceedings. University of Alaska Press: Fairbanks, pp. 125–130., 2008.
- Burton-Johnson, A., Black, M., Fretwell, P. T. and Kaluza-Gilbert, J.: An automated methodology for differentiating rock from snow, clouds and sea in Antarctica from Landsat 8 imagery: a new rock outcrop map and area estimation for the entire Antarctic continent, *The Cryosphere*, 10(4), 1665–1677, doi:https://doi.org/10.5194/tc-10-1665-2016, 2016.
- 20 Danielson, J. J. and Gesch, D. B.: Global multi-resolution terrain elevation data 2010 (GMTED2010), USGS Numbered Series, U.S. Geological Survey. [online] Available from: <http://pubs.er.usgs.gov/publication/ofr20111073> (Accessed 9 October 2018), 2011.
- Decker, E. R. and Bucher, G. J.: Geothermal studies in Antarctica, *Antarct. J. U. S.; (United States)*, 12:4 [online] Available from: <https://www.osti.gov/biblio/6112190> (Accessed 29 April 2019), 1977.
- 25 Dee, D. P., Uppala, S. M., Simmons, A. J., Berrisford, P., Poli, P., Kobayashi, S., Andrae, U., Balmaseda, M. A., Balsamo, G., Bauer, P., Bechtold, P., Beljaars, A. C. M., Berg, L. van de, Bidlot, J., Bormann, N., Delsol, C., Dragani, R., Fuentes, M., Geer, A. J., Haimberger, L., Healy, S. B., Hersbach, H., Hólm, E. V., Isaksen, L., Kållberg, P., Köhler, M., Matricardi, M., McNally, A. P., Monge-Sanz, B. M., Morcrette, J.-J., Park, B.-K., Peubey, C., Rosnay, P. de, Tavolato, C., Thépaut, J.-N. and Vitart, F.: The ERA-Interim reanalysis: configuration and performance of the data assimilation system, *Quarterly Journal of the Royal Meteorological Society*, 137(656), 553–597, doi:10.1002/qj.828, 2011.
- 30 Ferreira, A., Vieira, G., Ramos, M. and Nieuwendam, A.: Ground temperature and permafrost distribution in Hurd Peninsula (Livingston Island, Maritime Antarctic): An assessment using freezing indexes and TTOP modelling, *CATENA*, 149, 560–571, doi:10.1016/j.catena.2016.08.027, 2017.
- Fiddes, J. and Gruber, S.: TopoSCALE v.1.0: downscaling gridded climate data in complex terrain, *Geosci. Model Dev.*, 7(1), 387–405, doi:10.5194/gmd-7-387-2014, 2014.
- 35 Gallée, H.: Simulation of blowing snow over the antarctic ice sheet, *Annals of Glaciology*, 26, 203–206, doi:10.3189/1998AoG26-1-203-206, 1998.
- Gisnås, K., Etzelmüller, B., Farbrot, H., Schuler, T. V. and Westermann, S.: CryoGRID 1.0: Permafrost Distribution in Norway estimated by a Spatial Numerical Model, *Permafrost and Periglacial Processes*, 24(1), 2–19, doi:10.1002/ppp.1765,
40 2013.



- Gisnås, K., Westermann, S., Schuler, T. V., Litherland, T., Isaksen, K., Boike, J. and Etzelmüller, B.: A statistical approach to represent small-scale variability of permafrost temperatures due to snow cover, *The Cryosphere*, 8(6), 2063–2074, doi:10.5194/tc-8-2063-2014, 2014.
- Green, S. W., Gressitt, J. L., Koob, D., Llano, G. A., Rudolph, E. D., Singer, R., Steere, W. C. and Ugolini, F. C.: Terrestrial life of Antarctica. *Antarctic Map Folio Series*, Nat. Geogr. Soc. New York, 1967.
- 5 Guglielmin, M.: Ground surface temperature (GST), active layer and permafrost monitoring in continental Antarctica, *Permafrost and Periglacial Processes*, 17(2), 133–143, doi:10.1002/ppp.553, 2006.
- Guglielmin, M.: Advances in permafrost and periglacial research in Antarctica: A review, *Geomorphology*, 155–156, 1–6, doi:10.1016/j.geomorph.2011.12.008, 2012.
- 10 Guglielmin, M., Balks, M. R., Adlam, L. S. and Baio, F.: Permafrost thermal regime from two 30-m deep boreholes in southern victoria land, antarctica, *Permafrost and Periglacial Processes*, 22(2), 129–139, doi:10.1002/ppp.715, 2011.
- Guglielmin, M., Worland, M. R. and Cannone, N.: Spatial and temporal variability of ground surface temperature and active layer thickness at the margin of maritime Antarctica, Signy Island, *Geomorphology*, 155–156, 20–33, doi:10.1016/j.geomorph.2011.12.016, 2012.
- 15 Guglielmin, M., Worland, M. R., Baio, F. and Convey, P.: Permafrost and snow monitoring at Rothera Point (Adelaide Island, Maritime Antarctica): Implications for rock weathering in cryotic conditions, *Geomorphology*, 225, 47–56, doi:10.1016/j.geomorph.2014.03.051, 2014.
- Hersbach, H. and Dee, D.: ERA5 reanalysis is in production, *ECMWF Newsletter* 147, ECMWF., 2016.
- Hevesi, J. A., Istok, J. D. and Flint, A. L.: Precipitation Estimation in Mountainous Terrain Using Multivariate Geostatistics. Part I: Structural Analysis, *J. Appl. Meteor.*, 31(7), 661–676, doi:10.1175/1520-0450(1992)031<0661:PEIMTU>2.0.CO;2, 1992.
- 20 Hrbáček, F., Kňázková, M., Nývlt, D., Láška, K., Mueller, C. W. and Ondruch, J.: Active layer monitoring at CALM-S site near J.G.Mendel Station, James Ross Island, eastern Antarctic Peninsula, *Science of The Total Environment*, 601–602, 987–997, doi:10.1016/j.scitotenv.2017.05.266, 2017a.
- 25 Hrbáček, F., Nývlt, D. and Láška, K.: Active layer thermal dynamics at two lithologically different sites on James Ross Island, Eastern Antarctic Peninsula, *CATENA*, 149, 592–602, doi:10.1016/j.catena.2016.06.020, 2017b.
- Hrbáček, F., Láška, K. and Engel, Z.: Effect of Snow Cover on the Active-Layer Thermal Regime – A Case Study from James Ross Island, Antarctic Peninsula, *Permafrost and Periglacial Processes*, 27(3), 307–315, doi:10.1002/ppp.1871, 2016.
- 30 Hrbáček, F., Vieira, G., Oliva, M., Balks, M., Guglielmin, M., Pablo, M. Á. de, Molina, A., Ramos, M., Goyanes, G., Meiklejohn, I., Abramov, A., Demidov, N., Fedorov-Davydov, D., Lupachev, A., Rivkina, E., Láška, K., Kňázková, M., Nývlt, D., Raffi, R., Strelin, J., Sone, T., Fukui, K., Dolgikh, A., Zazovskaya, E., Mergelov, N., Osokin, N. and Miamin, V.: Active layer monitoring in Antarctica: an overview of results from 2006 to 2015, *Polar Geography*, 0(0), 1–15, doi:10.1080/1088937X.2017.1420105, 2018.
- 35 Humlum, O., Instanes, A. and Sollid, J. L.: Permafrost in Svalbard: a review of research history, climatic background and engineering challenges, *Polar Research*, 22(2), 191–215, doi:10.3402/polar.v22i2.6455, 2003.
- Kotzé, C. and Meiklejohn, I.: Temporal variability of ground thermal regimes on the northern buttress of the Vesleskarvet nunatak, western Dronning Maud Land, Antarctica, *Antarctic Science*, 29(1), 73–81, doi:10.1017/S095410201600047X, 2017.
- 40 Lacelle, D., Lapalme, C., Davila, A. F., Pollard, W., Marinova, M., Heldmann, J. and McKay, C. P.: Solar Radiation and Air and Ground Temperature Relations in the Cold and Hyper-Arid Quartermain Mountains, McMurdo Dry Valleys of Antarctica, *Permafrost and Periglacial Processes*, 27(2), 163–176, doi:10.1002/ppp.1859, 2016.



- Liston, G. E.: Representing Subgrid Snow Cover Heterogeneities in Regional and Global Models, *J. Climate*, 17(6), 1381–1397, doi:10.1175/1520-0442(2004)017<1381:RSSCHI>2.0.CO;2, 2004.
- Nylen, T. H., Fountain, A. G. and Doran, P. T.: Climatology of katabatic winds in the McMurdo dry valleys, southern Victoria Land, Antarctica, *Journal of Geophysical Research: Atmospheres*, 109(D3), doi:10.1029/2003JD003937, 2004.
- 5 Obu, J., Westermann, S., Bartsch, A., Berdnikov, N., Christiansen, H. H., Dashtseren, A., Delaloye, R., Elberling, B., Etzelmüller, B., Kholodov, A., Khomutov, A., Kääb, A., Leibman, M. O., Lewkowicz, A. G., Panda, S. K., Romanovsky, V., Way, R. G., Westergaard-Nielsen, A., Wu, T., Yamkhin, J. and Zou, D.: Northern Hemisphere permafrost map based on TTOP modelling for 2000–2016 at 1 km² scale, *Earth-Science Reviews*, 193, 299–316, doi:10.1016/j.earscirev.2019.04.023, 2019.
- 10 Oliva, M., Hrbacek, F., Ruiz-Fernández, J., de Pablo, M. Á., Vieira, G., Ramos, M. and Antoniades, D.: Active layer dynamics in three topographically distinct lake catchments in Byers Peninsula (Livingston Island, Antarctica), *CATENA*, 149, 548–559, doi:10.1016/j.catena.2016.07.011, 2017.
- Østby, T. I., Schuler, T. V. and Westermann, S.: Severe cloud contamination of MODIS Land Surface Temperatures over an Arctic ice cap, Svalbard, *Remote Sensing of Environment*, 142, 95–102, doi:10.1016/j.rse.2013.11.005, 2014.
- 15 de Pablo, M. A., Ramos, M. and Molina, A.: Thermal characterization of the active layer at the Linnopolar Lake CALM-S site on Byers Peninsula (Livingston Island), Antarctica, *Solid Earth*, 5(2), 721–739, doi:https://doi.org/10.5194/se-5-721-2014, 2014.
- de Pablo, M. A., Ramos, M. and Molina, A.: Snow cover evolution, on 2009–2014, at the Linnopolar Lake CALM-S site on Byers Peninsula, Livingston Island, Antarctica., *CATENA*, 149, 538–547, doi:10.1016/j.catena.2016.06.002, 2017.
- 20 Raffi, R. and Stenni, B.: Isotopic composition and thermal regime of ice wedges in northern Victoria Land, East Antarctica, *Permafrost and Periglacial Processes*, 22(1), 65–83, doi:10.1002/ppp.701, 2011.
- Ramos, M., Vieira, G., de Pablo, M. A., Molina, A., Abramov, A. and Goyanes, G.: Recent shallowing of the thaw depth at Crater Lake, Deception Island, Antarctica (2006–2014), *CATENA*, 149, 519–528, doi:10.1016/j.catena.2016.07.019, 2017.
- 25 Rocha, M. J., Dutra, E., Tomé, R., Vieira, G., Miranda, P., Fragoso, M. and Ramos, M.: ERA-Interim forced H-TESSEL scheme for modeling ground temperatures for Livingston Island (South Shetlands, Antarctic Peninsula), in *Proceedings of II Iberian Conference of the International Permafrost Association: Periglacial, Environments, Permafrost and Climate Variability: Colección Obras colectivas, Universidad de Alcalá.*, 2010.
- Romanovsky, V. E. and Osterkamp, T. E.: Interannual variations of the thermal regime of the active layer and near-surface permafrost in northern Alaska, *Permafrost and Periglacial Processes*, 6(4), 313–335, doi:10.1002/ppp.3430060404, 1995.
- 30 Schaefer, C. E. G. R., Michel, R. F. M., Delpupo, C., Senra, E. O., Bremer, U. F. and Bockheim, J. G.: Active layer thermal monitoring of a Dry Valley of the Ellsworth Mountains, Continental Antarctica, *CATENA*, 149, 603–615, doi:10.1016/j.catena.2016.07.020, 2017b.
- Schaefer, C. E. G. R., Pereira, T. T. C., Almeida, I. C. C., Michel, R. F. M., Corrêa, G. R., Figueiredo, L. P. S. and Ker, J. C.: Penguin activity modify the thermal regime of active layer in Antarctica: A case study from Hope Bay, *CATENA*, 149, 582–591, doi:10.1016/j.catena.2016.07.021, 2017a.
- 35 Shiklomanov, N. I.: From Exploration to Systematic Investigation: Development of Geocryology in 19th- and Early—20th-Century Russia, *Physical Geography*, 26(4), 249–263, doi:10.2747/0272-3646.26.4.249, 2005.
- Smith, M. W. and Riseborough, D. W.: Permafrost monitoring and detection of climate change, *Permafrost Periglac. Process.*, 7(4), 301–309, doi:10.1002/(SICI)1099-1530(199610)7:4<301::AID-PPP231>3.0.CO;2-R, 1996.
- 40 Smith, M. W. and Riseborough, D. W.: Climate and the limits of permafrost: a zonal analysis, *Permafrost Periglac. Process.*, 13(1), 1–15, doi:10.1002/ppp.410, 2002.



- Soliman, A., Duguay, C., Saunders, W., Hachem, S., Soliman, A., Duguay, C., Saunders, W. and Hachem, S.: Pan-Arctic Land Surface Temperature from MODIS and AATSR: Product Development and Intercomparison, *Remote Sensing*, 4(12), 3833–3856, doi:10.3390/rs4123833, 2012.
- 5 Vieira, G., Bockheim, J., Guglielmin, M., Balks, M., Abramov, A. A., Boelhouwers, J., Cannone, N., Ganzert, L., Gilichinsky, D. A., Goryachkin, S., López-Martínez, J., Meiklejohn, I., Raffi, R., Ramos, M., Schaefer, C., Serrano, E., Simas, F., Sletten, R. and Wagner, D.: Thermal state of permafrost and active-layer monitoring in the antarctic: Advances during the international polar year 2007–2009, *Permafrost and Periglacial Processes*, 21(2), 182–197, doi:10.1002/ppp.685, 2010.
- 10 Wan, Z.: New refinements and validation of the collection-6 MODIS land-surface temperature/emissivity product, *Remote Sensing of Environment*, 140, 36–45, doi:10.1016/j.rse.2013.08.027, 2014.
- Westermann, S., Østby, T. I., Gislås, K., Schuler, T. V. and Etzelmüller, B.: A ground temperature map of the North Atlantic permafrost region based on remote sensing and reanalysis data, *The Cryosphere*, 9(3), 1303–1319, doi:<https://doi.org/10.5194/tc-9-1303-2015>, 2015.
- 15 Zhang, Y., Olthof, I., Fraser, R. and Wolfe, S. A.: A new approach to mapping permafrost and change incorporating uncertainties in ground conditions and climate projections, *The Cryosphere*, 8(6), 2177–2194, doi:10.5194/tc-8-2177-2014, 2014.